OH* CHEMILUMINESCENCE: PRESSURE DEPENDENCE OF

O + H + M = OH* + M

A Thesis

by

NICOLE DONATO

Submitted to the Office of Graduate Studies of
Texas A&M University
in partial fulfillment of the requirements for the degree of

MASTER OF SCIENCE

December 2009

Major Subject: Mechanical Engineering

OH* CHEMILUMINESCENCE: PRESSURE DEPENDENCE OF

$O + H + M = OH^* + M$

A Thesis

by

NICOLE DONATO

Submitted to the Office of Graduate Studies of
Texas A&M University
in partial fulfillment of the requirements for the degree of

MASTER OF SCIENCE

Approved by:

Chair of Committee,	Eric Petersen
Committee Members,	Bing Guo
	Sai Lau
Head of Department,	Sai Lau

December 2009

Major Subject: Mechanical Engineering

ABSTRACT

OH* Chemiluminescence: Pressure Dependence of O + H + M = OH* + M.

(December 2009)

Nicole Donato, B.S., University of Central Florida

Chair of Advisory Committee: Dr. Eric L. Petersen

The measure of chemiluminescence from the transition of the hydroxyl radical from its electronically excited state ($A^2\Sigma^+$) to its ground state ($X^2\Pi$) is used in many combustion applications for diagnostic purposes due to the non-intrusive nature of the chemiluminescence measurement. The presence of the ultraviolet emission at 307nm is often used as an indicator of the flame zone in practical combustion systems, and its intensity may be correlated to the temperature distribution or other parameters of interest. To date, the measurement of the excited state OH, OH*, is mostly qualitative. With the use of an accurate chemical kinetics model, however, it is possible to obtain quantitative measurements.

Shock-tube experiments have been performed in highly diluted mixtures of $H_2/O_2/Ar$ at a wide range of pressures to evaluate the pressure-dependent rate coefficient of the title reaction. In such mixtures the main contributing reaction to the formation of OH* is,

$$O + H + M = OH^* + M. \qquad R1$$

Previous work has determined the reaction rate of R1 at atmospheric conditions and accurately predicts the amount of OH* experimentally produced. At elevated pressures up to 15 atm, which are of interest to the gas turbine community, the currently used reaction rate of R1 (i.e., without any pressure dependence) significantly over predicts the amount of OH* formed. This work provides the pressure dependence of R1. The new reaction rate is able to reproduce the experimental data over the range of conditions studied and enables quantitative measurements applicable to practical combustion environments.

ACKNOWLEDGMENTS

First and foremost I would like to thank my advisor, Dr. Petersen. Leading by example, his work ethic has been a source of inspiration throughout my research. I would also like to thank my committee members, Dr. Guo, and Dr. Lau, for their support.

Thanks also go to my colleagues and the department faculty and staff for making my time at Texas A&M University a great experience. Finally, thanks to my family and friends for their encouragement, patience and love.

NOMENCLATURE

OH*	Electronically excited hydroxyl radical
OH(X)	Ground-state hydroxyl radical
ϕ	Fuel/oxidizer equivalence ratio
ki	Reaction rate coefficient
Ri	Number of the i^{th} elementary reaction
A	Pre-exponential factor in the Arrhenius expression for a rate coefficient
n	Temperature exponent in the Arrhenius expression
E	Activation of the elementary reaction (cal/mol)
R	Universal gas constant
[X]	Concentration of species X
t	Experimental time (μs)

TABLE OF CONTENTS

Page

Page

LIST OF FIGURES

Page

Page

LIST OF TABLES

Page

CHAPTER I

INTRODUCTION

Chemiluminescence, an optical signature of the combustion process, offers unique diagnostic capabilities due to the relatively inexpensive and nonintrusive nature of the chemiluminescence measurement. Ultraviolet emission at 307nm, due to the transition of the hydroxyl radical from its electronically excited state ($A^2\Sigma^+$) to its ground state ($X^2\Pi$), has long been recognized as a diagnostics method in many combustion applications. Several studies have shown the ratio of peak OH*/CH* chemiluminescence provides key insight to a flame's heat release rate, temperature distribution, local equivalence ratio, and degree of mixing [1-9].

Chemiluminescence measurements are extremely useful in practical combustion applications, but they are qualitative in nature, lacking a direct relationship between recorded intensity and absolute concentration of the emitting species. If the detailed kinetics modeling of the OH* chemistry is well known, however, calibration can still be accomplished. Kinetics modeling of OH* requires knowledge of the elementary reactions that form and quench the excited-state hydroxyl radical as well as their rate coefficients. Many previous studies have identified the relevant reactions and their rates [10-41].

The result of these works have found the main reactions in hydrogen mixtures

---

This thesis follows the style of *AIAA*.

leading to the formation and quenching of OH* are

$$O + H + M = OH^* + M \qquad R1$$

$$OH^* + M = OH + M \qquad R2\text{-}9$$

$$OH^* = OH + h\nu \qquad R10$$

where M represents the possible colliding molecules (Ar, H_2O, H_2, O_2, OH, H, O, and N_2). This work uses the reaction rate for R1 from the recent work of Hall et al [30], which was validated at low-pressure conditions. Table 1 shows the reactions and rates from Hall and coworkers with the addition of R9 taken from Tamura et al. [37].

Table 1. Elementary reactions that model OH* formation and quenching. Rate coefficients are expressed as $k = AT^n\exp(-E/RT)$ with units of cal, mol, cm, and s.

#	Reaction	A	n	E	Source	Ref#
1	$O + H + M = OH^* + M$	3.1×10^{14}	0.0	10,000	Hall et al.	[30]
2	$OH^* + AR = OH + AR$	2.17×10^{10}	0.5	2060	Paul et al.[1]	[28]
3	$OH^* + H_2O = OH + H_2O$	5.92×10^{12}	0.5	-861	Tamura et al.	[37]
4	$OH^* + H_2 = OH + H_2$	2.95×10^{12}	0.5	-444	Tamura et al.	[37]
5	$OH^* + O_2 = OH + O_2$	2.10×10^{12}	0.5	-482	Tamura et al.	[37]
6	$OH^* + OH = OH + OH$	1.50×10^{12}	0.5	0.0	Hidaka et al.	[26]
7	$OH^* + H = OH + H$	1.50×10^{12}	0.5	0.0	Hidaka et al.	[26]
8	$OH^* + O = OH + O$	1.50×10^{12}	0.5	0.0	Hidaka et al.	[26]
9	$OH^* + N_2 = OH + N_2$	1.08×10^{11}	0.5	-1238	Tamura et al.	[37]
10	$OH^* = OH + h\nu$	1.40×10^{6}	0.0	0.0	German et al.	[38]

[1] The value for quenching by Ar was reported by Paul et al. [28] as an upper limit, and is used herein as the nominal value for this rate.

Many practical combustion systems operate at elevated pressures. While the Hall et al. OH* mechanism accurately predicts the peak formation of OH* at atmospheric conditions, it is virtually untested at elevated pressures. There is no reason to expect the 1-atm rate coefficient for R1 to be valid at elevated pressures because the use of the collider species M infers that there is some dependence on the pressure. In fact, as is shown later in this thesis, the 1-atm reaction rate significantly over predicts the peak at higher pressures. Prior to this thesis, there exist no rate coefficient measurements or estimates for R1 at pressures above 1 atm. Thus it is necessary to perform experiments at a range of pressures (1, 10, and 15 atm) to improve the peak amount of OH* predicted by the kinetics mechanism at practical turbine conditions.

This thesis will provide an overview of relevant contributing works available in the literature, followed by a brief review of kinetic and Lindemann theory. Next, the experimental apparatus and kinetics modeling used in this wok will be discussed at length. Additionally, details on the pressure excursion will be provided as well as a discussion on the ultimate pressure dependence developed. Finally, the last chapter provides conclusions and points out further avenues for future experimental investigations on the pressure dependence of R1.

CHAPTER II

LITERARY SEARCH AND BACKGROUND

Literary Search

OH* emission measurements have been shown to provide a cost effective, nonintrusive method for observing the combustion processes occurring in many practical systems. Several studies have shown that the ratio of peak OH*/CH* chemiluminescence provides key insight to a flame's heat release rate, temperature distribution, local equivalence ratio, and degree of mixing. Both Higgins et al [1] and Docquier et al. [2] have shown that OH chemiluminescence measurements can be used for active-control systems, while Hardalupas and Orain [3], Muruganandam et al. [4], Nori and Seitzman [5], and Kojima et al. [6] have demonstrated the link between the ratio of peak OH*/CH* chemiluminescence to the fuel-air equivalence ratio. A fast-response chemiluminescent flame detection approach was presented by Roby et al. [8], and Edwards et al. [9] showed the temperature in a $H_2/O_2/Ar$ shock-heated gas could be calculated using the ratio of observed intensities. OH* emission has long been used as a marker of ignition in shock-tube studies, and the recent work of Petersen [42] detailed its proper use in defining ignition delay times.

Suggestions for the reactions forming OH* date back to those offered by Gaydon and coworkers [10,11]. Since then, many flame studies have been conducted looking at OH* chemiluminescence including work done in the 1950s by Charton and Gaydon [11],

and Kaskan [12]. More recently, Smith et al. [17] presented a full set of OH* reactions and rates. Over the years, many shock-tube studies have been performed to examine OH* emission. Belles and Lauver [23], Gutman et al. [24], Gardiner et al. [25], Hidaka et al. [26], Koike and Morinaga [27], Paul et al. [28], Petersen et al. [29], Hall et al. [30], and recently Kathrotia et al. [31] all studied hydrogen mixtures in shock tubes. The low-pressure reaction rate for R1: O + H + M = OH* + M has been studied by a handful of authors [18],[26],[27],[30],[31]. The reaction rate suggested for R1 differs by two orders of magnitude from each other. Hidaka et al. [26] recommended the lowest rate of reaction to be $1.2x10^{13}exp(-6840/RT)$, while Hall et al. recommended the highest rate of reaction, $3.1x10^{14}exp(-10000/RT)$. Regardless of reaction rate used, all of the suggested rates inaccurately predict the peak OH* formed at elevated pressures. The OH* mechanism by Hall et al. [30] serves as the base low-pressure OH* mechanism for the work herein. OH* formation rates have also been examined in hydrocarbon mixtures by Carl et al. [32], which were taken at temperatures below 511K, Grebe and Homann [33], Porter et al. [34], and Marques et al. [35]. Skrebkov et al. [36] studied the formation mechanism of OH* by a theoretical *ab-initio* analysis. The non-reactive collisional quenching of OH*, where excited state OH* transfers its excess energy to a colliding molecule, has been well studied [26,28,37] and is fixed at established literature values for this study.

Kinetics Theory

Experimentally obtained reaction rates for the elementary reaction forming OH* at high temperatures and elevated pressures is the goal of the present work. This section reviews the reaction kinetic theory relevant to rate coefficients.

In a global reaction of some fuel with an oxidizer, the initial reactants ultimately form the final products. The actual conversion of reactants to products is made up of many elementary reactions and takes some finite amount of time. Each elementary reaction occurs at different rates that are functions of temperature and sometimes pressure. A single elementary reaction rate is characterized by its rate coefficient, k, which is given by 3 parameters, A, n, and E in the following form:

$$k = AT^{n}\exp\left(\frac{-E}{RT}\right)$$

where A is the pre-exponential factor, n is the temperature exponent and E is known as the activation energy. The complete set of elementary reactions and their corresponding reaction parameters that describe the global reaction is called a mechanism.

As in this work, it is often of interest to examine the concentration of some species as a function of time. A given species concentration can be written as a differential equation in terms of the reactions that form and consume the species. Each term of the equation is made of the product of the rate coefficient, k, and the concentration of the reactant species. A term is positive if the reaction forms the species of interest and negative if it consumes the species.

Lindemann Theory

Under certain conditions, some reaction rate expressions depend on pressure as well as temperature. One of the first explanations for the pressure dependence of these reactions was presented by Lindemann in 1922 [43,44]. From Lindemann theory, the overall rate coefficient, k, is a combination of a low-pressure limit and a high-pressure limit. Lindemann suggested the overall reaction process as

$$R + M \xrightarrow{k_{1,f}} R^{\#} + M$$

$$R^{\#} + M \xrightarrow{k_{1,b}} R + M$$

$$R^{\#} \xrightarrow{k_2} P$$

where $R^{\#}$ is the excited intermediate species. Applying the quasi steady state approximation for $R^{\#}$, the reaction rates can be written as

$$\frac{\partial[R]}{\partial t} = -k_{1,f}[R][M] + k_{1,b}[R^{\#}][M]$$

$$\frac{\partial[R^{\#}]}{\partial t} = k_{1,f}[R][M] - k_{1,b}[R^{\#}][M] - k_2[R^{\#}] = 0$$

After some algebra, the reaction rate, $\frac{\partial[R]}{\partial t}$, can be written as:

$$\frac{\partial[R]}{\partial t} = \left[\frac{-k_{2,f}\left(k_{1,f}/k_{1,b}\right)}{1 + \left(k_2/k_{1,b}\right)[M]}\right][R]$$

For a unimolecular reaction,

$$\frac{\partial[R]}{\partial t} = -K[R]$$

Thus,

$$K = \left[\frac{-k_{2,f}\left(k_{1,f}/k_{1,b}\right)}{1 + \left(k_2/k_{1,b}\right)[M]}\right]$$

where [M] = P/RT and R is the universal gas constant. At the high-pressure limit, P → ∞, and [M] → ∞, so the rate constant is independent of pressure,

$$k_\infty = k_2\left(k_{1,f}/k_{1,b}\right)$$

At the low-pressure limit, P→ 0, and [M] → 0, thus the rate constant is directly proportional with pressure,

$$k_{low} = k_{1,f}[M]$$

were,

$$k_{1,f} = AT^n \exp\left(\frac{-E}{RT}\right)$$

From Lindemann theory, a log-log plot of the unimolecular rate constant is shown in Figure 1. The area between the high- and low-pressure regimes is known as the falloff regime.

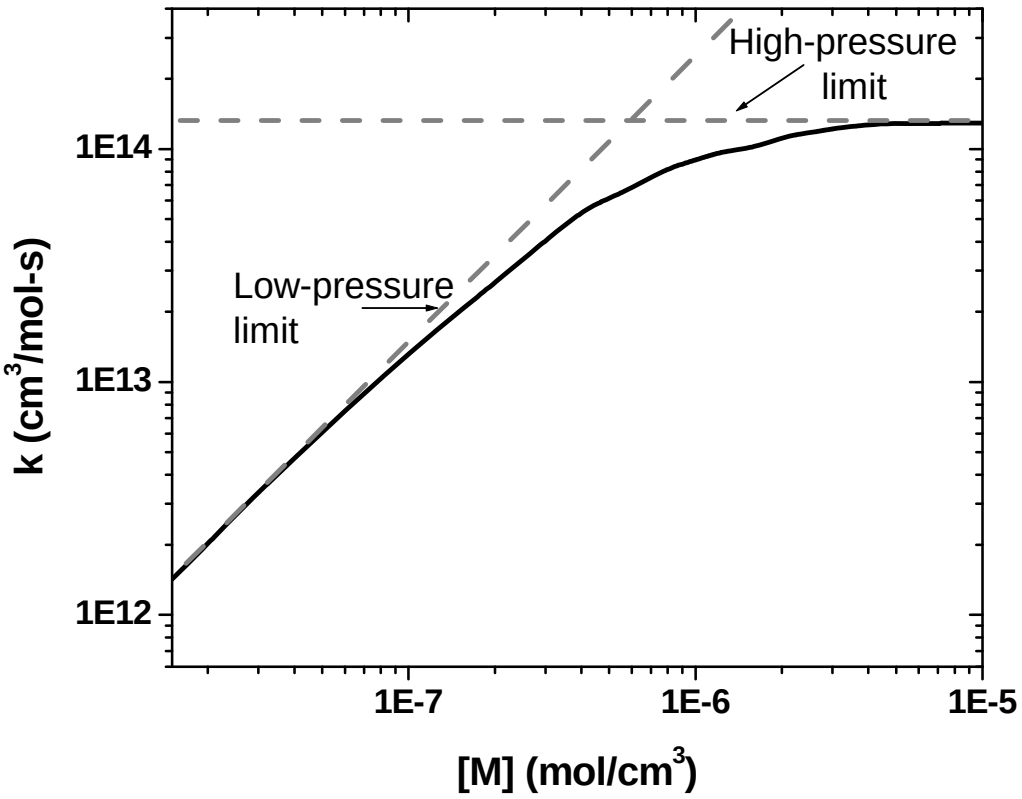

Figure 1. The Lindemann plot shows pressure range where the rate goes from the high-pressure regime (independent of pressure) to the low-pressure regime (rate proportional to total pressure). K is written for a reaction in the bimolecular form of A + B → C.

CHAPTER III

EXPERIMENTAL SETUP AND MODELING

Shock-Tube Experimental Setup

Shock tubes, due to their highly repeatable test conditions and uniform flow fields, have been used for several decades to study high-temperature chemical kinetics. A shock-tube facility capable of achieving the elevated pressures and temperatures needed for the present study is described in this section. The incident-shock velocity at the test region is used to determine the overall conditions behind the reflected shock by way of one-dimensional shock relations. The incident-shock measurement is facilitated by five pressure transducers (PCB 113) set in series along the side of the shock tube, which feed signals to four Fluke PM 6666 timer counter boxes that provide the time of passage between each pressure transducer. The inferred velocities for increment are in turn used to extrapolate the incident-shock velocity directly to the end wall.

The shock-tube facility, presented by Aul et al. [45], has driven-section length and inner diameter dimensions of 4.72 m and 15.24 cm, respectively, and a driver section length and an inner diameter of 4.93 m and 7.62 cm, respectively. A schematic of the facility is shown in Figure 2. The shock tube is constructed entirely of 304 stainless steel.

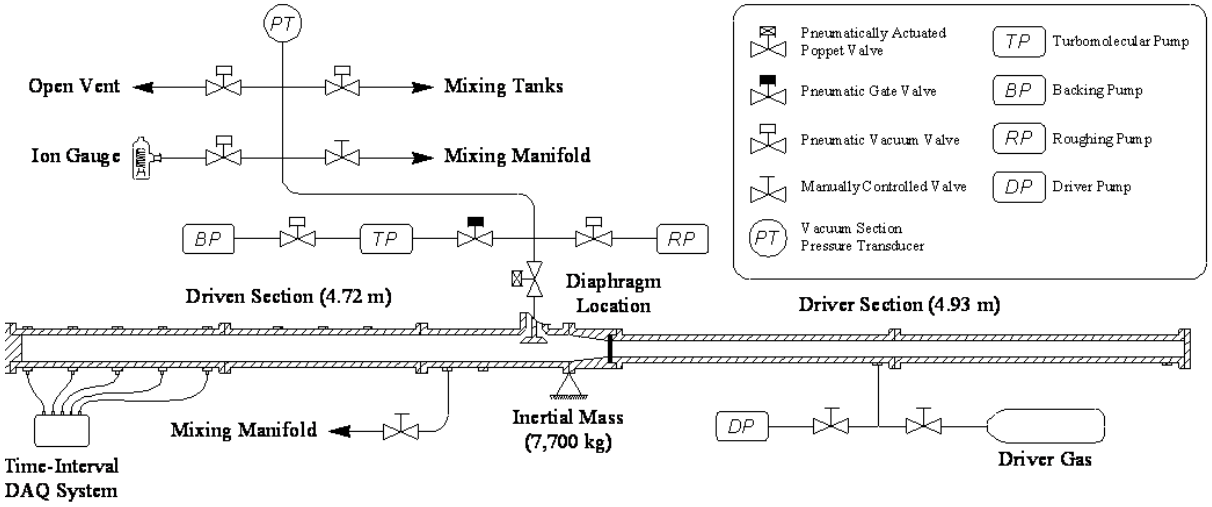

Figure 2. Schematic of shock-tube facility presented in Aul et al. [45].

Emission measurements of OH* chemiluminescence are made at the sidewall location, 1.6 cm from the end wall, through CaF_2 windows. The light from the windows is then passed through a 1-mm slit and focused onto a 307±5 nm bandpass filter in sequence with a Hamamatsu 1P21 photomultiplier tube (PMT) in a home-made housing, as seen in Figure 3. A vertically oriented slit, approximately 1 mm wide, was used to provide an optimal balance between strength and resolution of the recorded signal. The PMT had been previously optimized to maintain linearity of output voltage with respect to input signal; all experiments were performed at conditions selected to produce peak voltages within the range of PMT linearity [46]. In order to compare recorded OH* profiles, identical optical settings were maintained throughout the series of experiments. Care was taken to ensure that the optical equipment was not disturbed. Each of the data signals is processed

through a 14-bit GageScope digital oscilloscope board with sampling rates of 1 MHz or greater per channel.

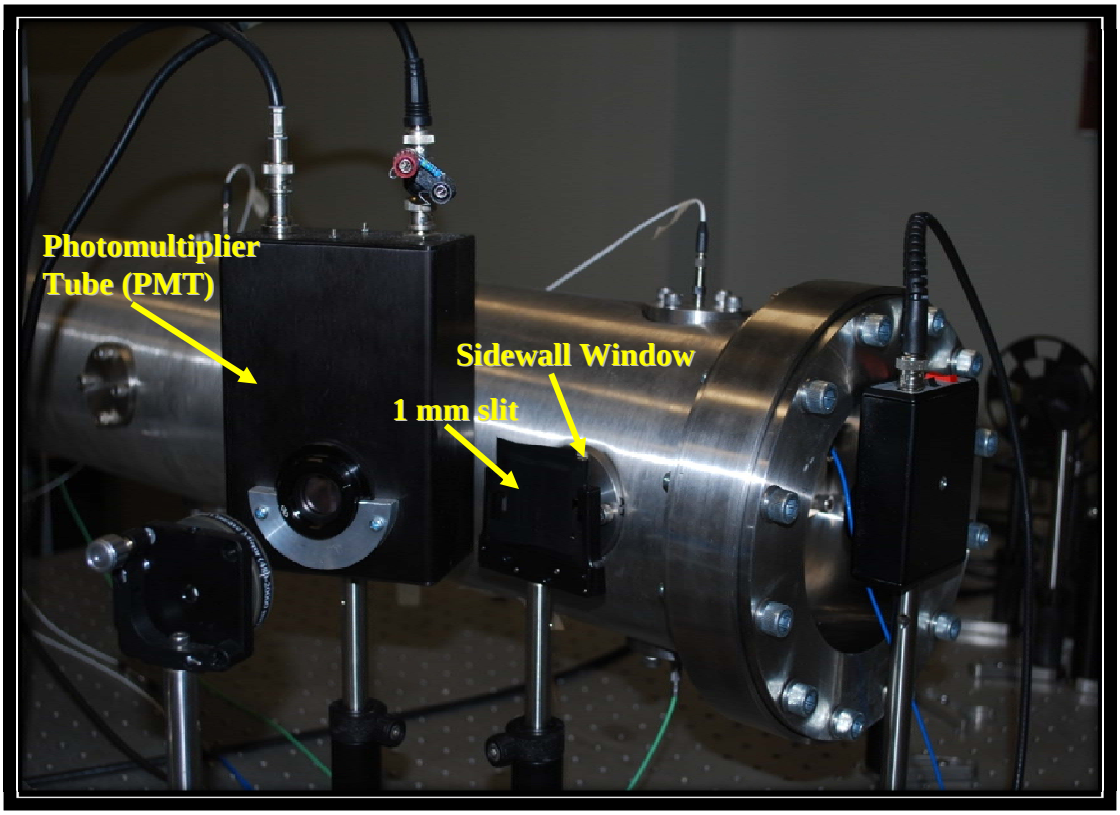

Figure 3. Photograph noting important OH* chemiluminescence diagnostics located near the endwall of the shock-tube.

Ultra-high purity (UHP, 99.9995%) argon, hydrogen, and oxygen were used to prepare the test mixtures. Dilution levels were maintained at 98.5% Ar to minimize heat release and pressure rise due to combustion. Argon was used as the diluent so that pressure and temperature remain constant at the test conditions, allowing accurate modeling using the

chemistry mechanism. Table 2 lists the mixtures used in this study to determine the pressure dependence of R1.

Table 2. Mixture compositions used for OH* chemiluminescence experiments.

Target Pressure	ϕ	$\%C_9H_{20}$	$\%O_2$	%Ar	Purpose
1	1.0	1.0	0.5	98.5	Pressure dependence of R1
10	1.0	1.0	0.5	98.5	Pressure dependence of R1
15	1.0	1.0	0.5	98.5	Pressure dependence of R1
1	1.0	2.0	1.0	97.0	Calibration curve

Chemical Kinetics Modeling

The Chemkin software collection [47] was used to perform the kinetics calculations using the homogenous batch reactor routine assuming constant volume and constant internal energy. At the dilute conditions of this study, there is little difference between an assumption of constant volume and one of constant pressure. The detailed H_2 chemistry was modeled using the Gas Research Institute's GRI-Mech 3.0 [48]. While there are multiple H_2 chemistry mechanisms available in literature since the introduction of GRI-Mech 3.0, the GRI mechanism was chosen because it has been well validated for dilute mixtures such as the one in this study. The Ó Conaire hydrogen submechanism from the University of Ireland, Galway [49] was also considered for use since it has been well validated over a wide range of conditions [50-55]. However, comparing predicted

OH* profiles, GRI-Mech 3.0 does a better job than the Ó Conaire mechanism at these dilute conditions in matching the shape of the experimentally obtained profiles as seen in Figure 4 for 1498 K, 1.3 atm. The complete list of species and reactions used in GRI-Mech 3.0 are listed in Appendix A and B respectively. The thermodynamic data for OH* were updated to reflect the most recent value for the heat of formation obtained from the Burcat thermodynamics database [56].

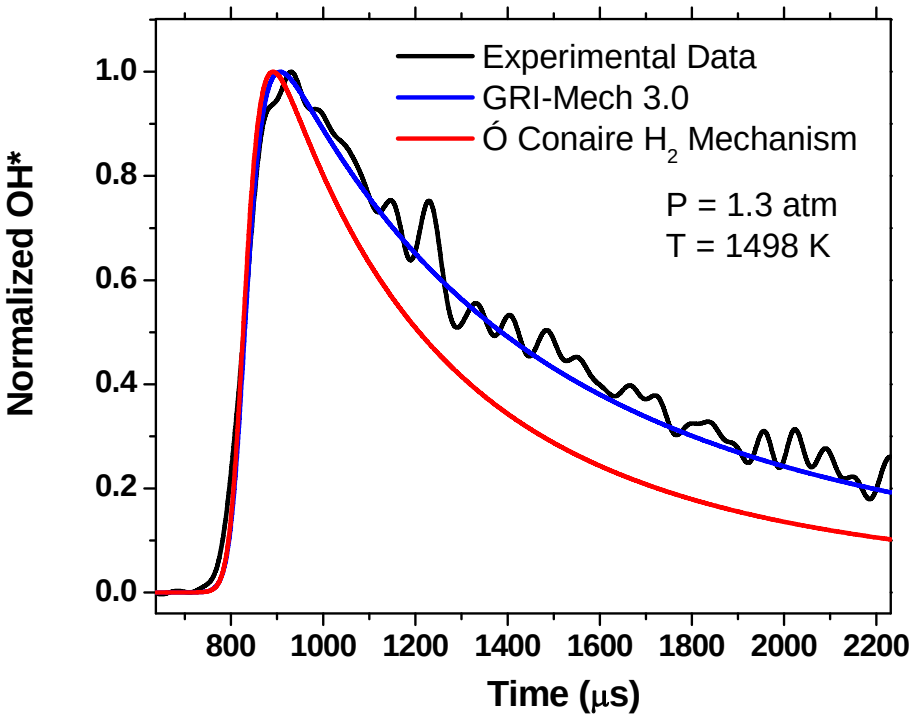

Figure 4. Normalized model predictions from GRI Mech-3.0 agree much better with experimentally obtained OH* profiles than the Ó Conaire hydrogen mechanism, shown here for 1498 K and 1.3 atm. Such agreement is representative of all low-pressure conditions. Times have been shifted to align OH* profiles.

As mentioned in Chapter I, the formation and depletion of OH* are modeled by the following elementary reactions:

$$O + H + M = OH^* + M \qquad R1$$

$$OH^* + M = OH + M \qquad R2\text{-}9$$

$$OH^* = OH + h\nu \qquad R10$$

where M represents the colliding molecules (Ar, H_2O, H_2, O_2, OH, H, O, and N_2). For the temperatures examined in this study (T < 2300 K), R1 is the main reaction leading to the formation of OH*. R2-9 and R10 are the main reactions responsible for bringing the excited state OH* back to its ground state, OH(X). Studies have shown that at temperatures above 2800K, R1 works in reverse to deplete OH*, while thermal excitation causes the quenching reactions, R2-9, to work in reverse forming OH*. Figure 5a shows the modeling results for the hottest temperature case examined in the present study where OH* concentration is plotted as a function of time. It can be seen that the peak [OH*] (mol/cm^3) does not differ appreciably if the quenching reverse reactions rates are turned off or left on. At temperatures above 2800 K, as seen in Figure 5b, leaving the quenching reaction reverse rates on yields a greater concentration of OH*. Thus, for the conditions (T < 2300 K) of this study the main reaction contributing to OH* formation is indeed R1.

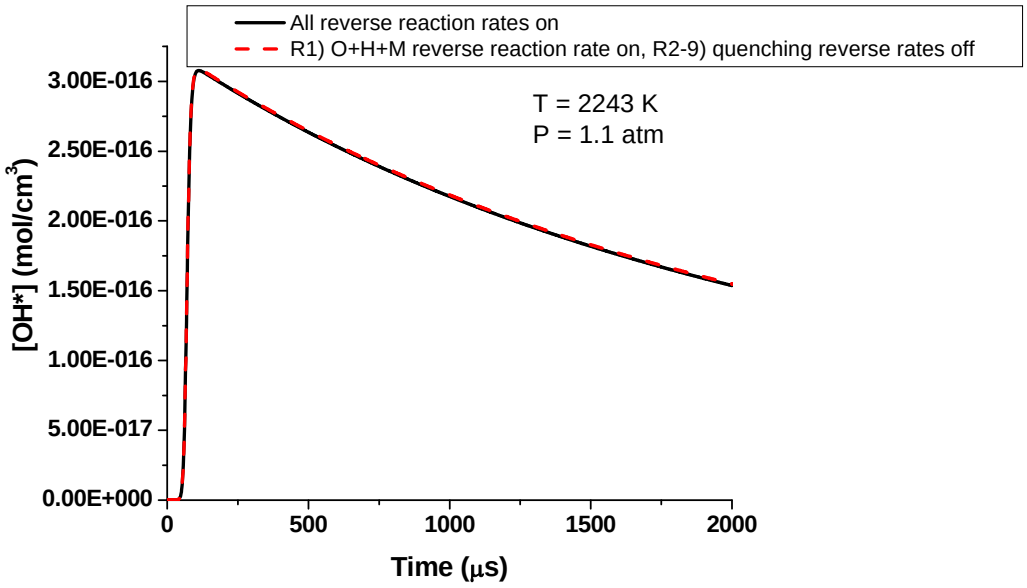

(a) Modeling results for T = 2243 K, 1.1 atm, which is the hottest temperature examined in this study.

Figure 5. Peak OH* concentration is determined by the formation reaction, R1 at 2243K and is not affected by the reverse quenching reactions at the highest temperature in this study.

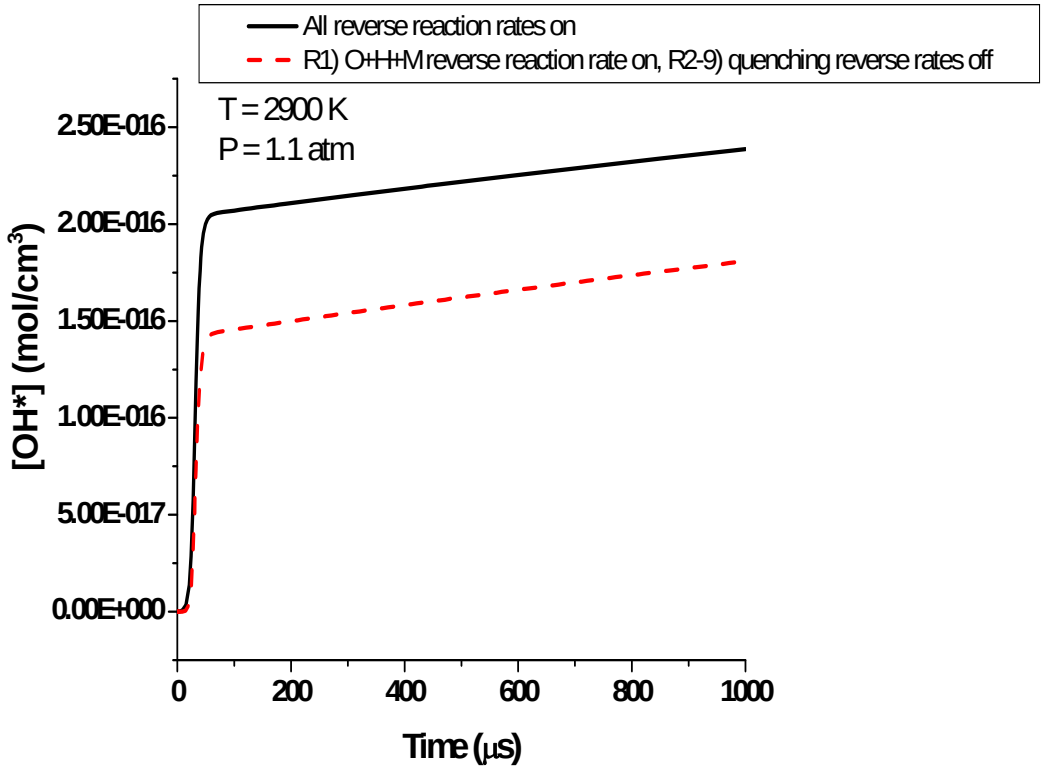

(b) At 2900 K, 1.1 atm, the quenching reactions work in the reverse direction to produce more OH*.

Figure 5 continued

Before an accurate OH* kinetics model can be developed for high-pressure conditions, it is necessary to start with a good low-pressure model. The detailed work of Hall et al. [30] included shock-tube experiments and utilized a fitting parameter approach to derive the rate of reaction of R1 at atmospheric conditions. Hall's work serves as the basis for the pressure excursion in this study. Hall determined the reaction rate of R1 to

be $3.1\times10^{14}\exp(-10000/RT)$ $cm^6mol^{-2}s^{-1}$. The quenching reactions used in the Hall mechanism came from established values in the literature [18,26,28,37,38] and are the same in this study. When deciding on the final base OH* mechanism, it was decided to leave the reverse rates of all reactions on.

CHAPTER IV

PRESSURE EXCURSION

Once the optimal settings were obtained and experiments underway, it was necessary to validate the results with other data available in the literature. Petersen et al. [29] performed shock-tube experiments using the same mixture of $H_2/O_2/Ar$ with 98.5% dilution, $\phi = 1.0$, to examine the chemical kinetics of OH* ($A^2\Sigma^+ - X^2\Pi$) chemiluminescence in the temperature range from 1010 -1750 K at low pressure. The shock tube used in the study by Petersen et al. [29] is similar to the one used in this study and is detailed in [57]. Since the optical settings differ between sets of experiments, it is necessary to normalize the data to a particular temperature and pressure, thus enabling a direct comparison of the data. A set of date were taken with the current setup to compare directly with the earlier data, and Figure 6 verifies the repeatability of the low-pressure experimental results obtained by Petersen and co-workers. For good measure, the experimentally obtained OH* profiles of this study were also compared to those of Petersen et al. [29] for cases of similar temperature. Figure 7 shows general agreement in the shape of the profiles between experiments. Slight differences can be attributed to the difference in temperature and the difference in optical settings. With low-pressure experiments validated against established data available in literature, the next major step was to perform a pressure excursion at 10 and 15 atm to obtain high-pressure data for the study herein.

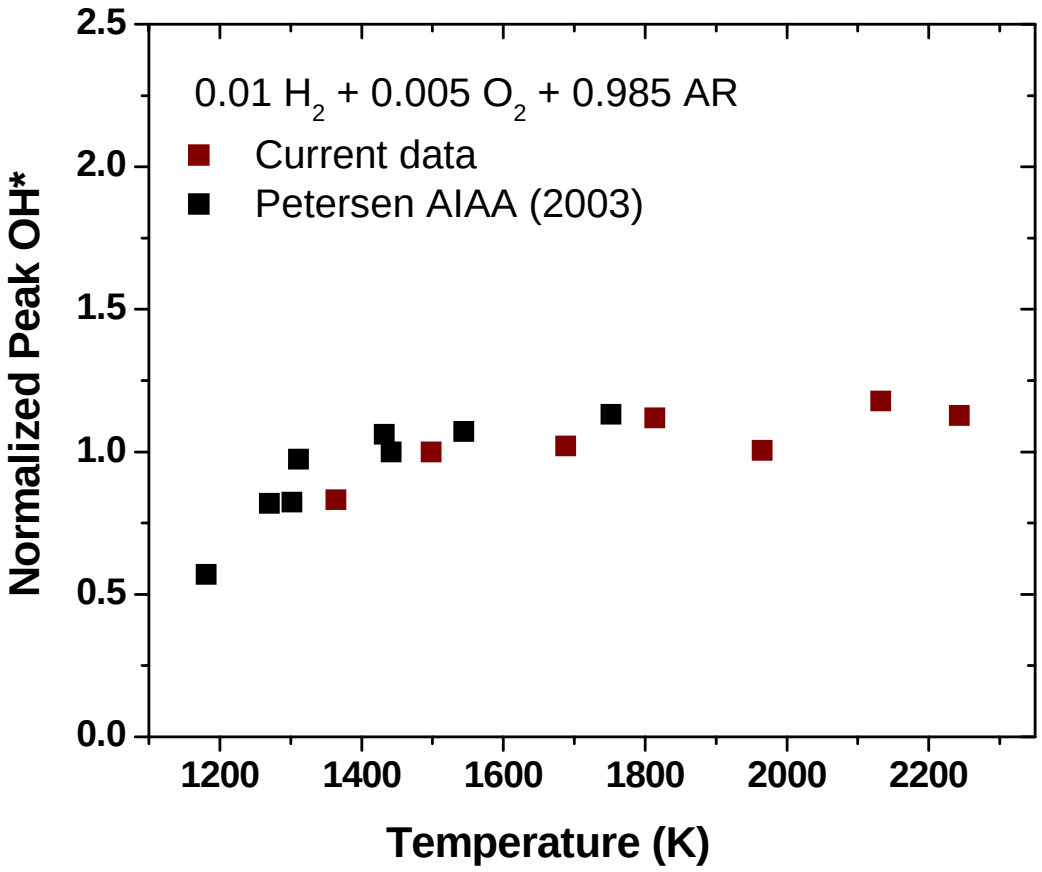

Figure 6. Maximum OH* concentration as a function of temperature at constant pressure and optical settings compared to the work of Petersen et al. [29]. Peak values are normalized to 1498 K and 1.15 atm.

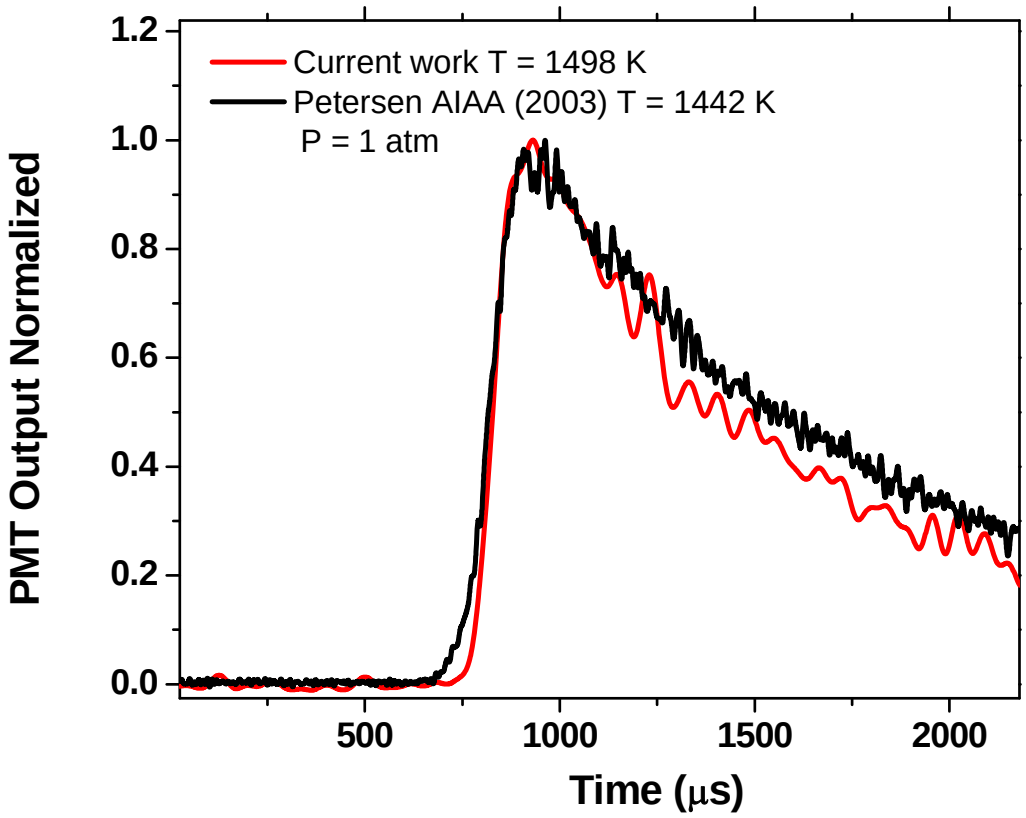

Figure 7. The normalized, experimentally obtained profile of OH* agrees well with the profile from Petersen et al. [29] at atmospheric conditions. Times have been adjusted to align OH* for comparison purposes.

As previously stated, the qualitative measurement of OH* chemiluminescence does not give a direct measure of the OH* concentration (mol/cm^3). PMT output and OH* concentration are, however, proportional. Since the kinetics modeling of OH* at atmospheric pressure is well known [30], a calibration curve can be established using 1-atm experiments to extrapolate at conditions outside the range where the model has been

verified. The calibration curve relates the PMT output (mV) to absolute concentration (mol/cm^3). A second set of low-pressure experiments was performed to cover a wide enough range of PMT output to create the calibration curve. The calibration mixture was $H_2/O_2/Ar$, $\phi = 1.0$ with 97% dilution, as opposed to 98.5% Ar dilution used in the rest of this work. The PMT output remains in the linear range, as determined by [46], so and the concentration is directly proportional to the emission intensity, so extrapolation of the curve up to 700 mV is justified. The results of the calibration can be seen in Figure 8. The calibration curve used to obtain absolute [OH*] (mol/cm^3) from the PMT output voltage is:

$$[OH*] = -1.217 \times 10^{-16} + \{(4.899 \times 10^{-17}) \times PMT\ output\}$$

where OH* is in mol/cm^3 and PMT output is in mV.

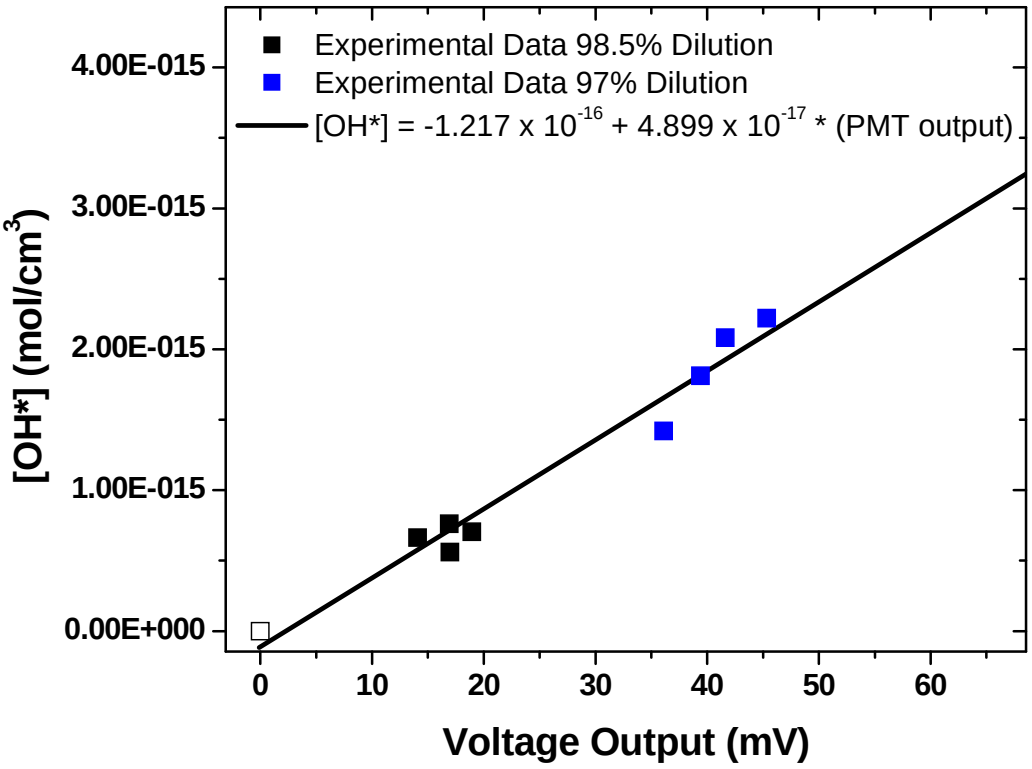

Figure 8. Calibration curve used to calibrate PMT output (mV) to OH* concentration (mol/cm^3).

Finally, high-pressure experiments were performed at 10 and 15 atm over a wide range of temperatures. Comparisons of the experimental results to original model predictions are shown in Figure 9. Error bars are shown in Figure 9 to represent the uncertainty in the value of the peak magnitude due to experimental repeatability from test to test, and was determined to be 10%. An uncertainty of ±10 K is associated with the experimental temperature determination. Although the model does a good job of predicting peak OH* formation at atmospheric pressure as expected, it significantly over

predicts the peak concentration at higher pressures (10 and 15 atm). The model also shows a different trend than the data at the highest temperatures by predicting a decrease in peak OH*. In the following chapter, the experimental data are used to obtain an improved model at elevated pressures.

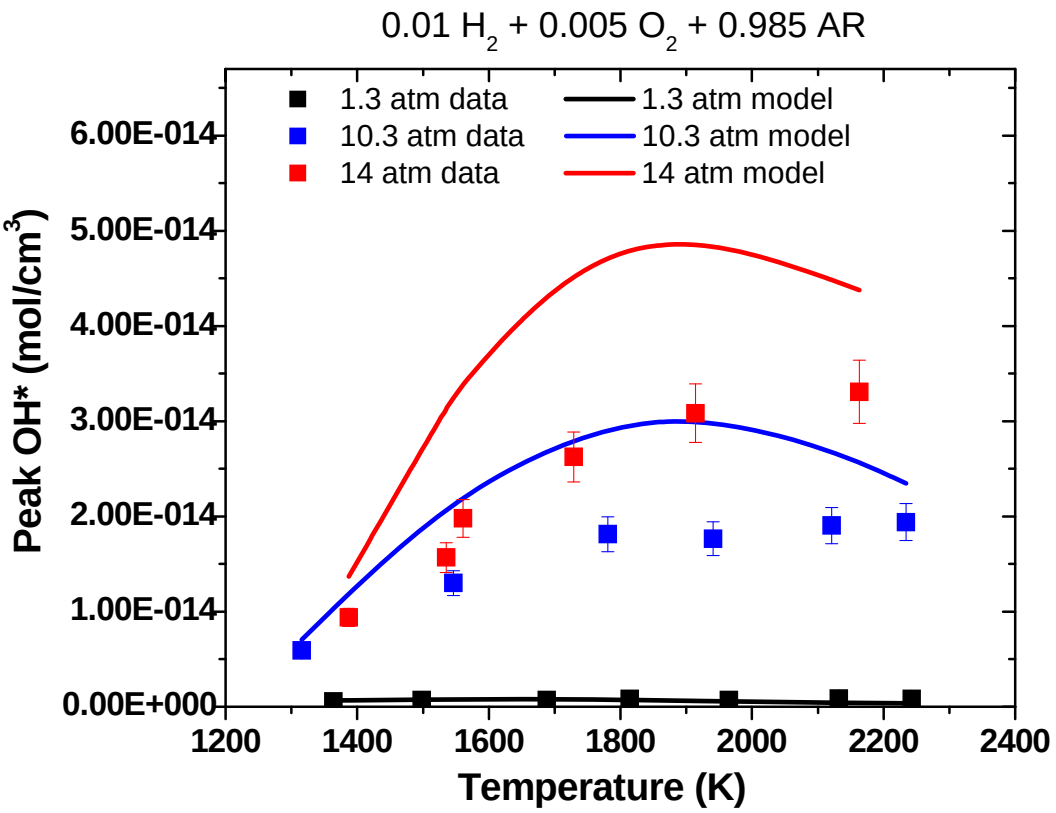

Figure 9. The original model predictions (lines) significantly over predict the experimental results at elevated pressures.

CHAPTER V

PRESSURE DEPENDENCE AND DISCUSSION

Before any steps were taken to improve the model, a local sensitivity analysis was performed on OH* to determine the most influential reaction(s) at the peak of the OH* curve. Sensitivity coefficients are given as the change in OH* concentration due to the change in rate of the given reaction. Figure 10 is a representative case where the local sensitivity analysis was performed at 1546 K, 10.3 atm. Positive values on the sensitivity plot lead to increased production of OH*, where negative values lead to the destruction of OH*. The onset of OH* formation is dominated by the main H_2/O_2 chemistry as seen by the chain branching reactions, which are assumed to be well known in this study and were not adjusted:

$$H + O_2 = O + OH$$

$$O + H_2 = H + OH$$

The most sensitive reaction to at the peak of the OH* concentration profile, however, is

$$O + H + M = OH^* + M \qquad \text{R1}$$

Additionally, the quenching reactions, R2 and R3, show up as slightly sensitive at the peak of OH*. Since the quenching rates are fixed at their literature values, and are not nearly as sensitive near the peak as R1, the magnitude of the peak height was used to obtain the rate of the reaction for R1 since the rate of this reaction dominates the OH* kinetics at the time of peak OH*. The sensitivity results shown in Figure 10 are representative of the entire range of conditions in this study.

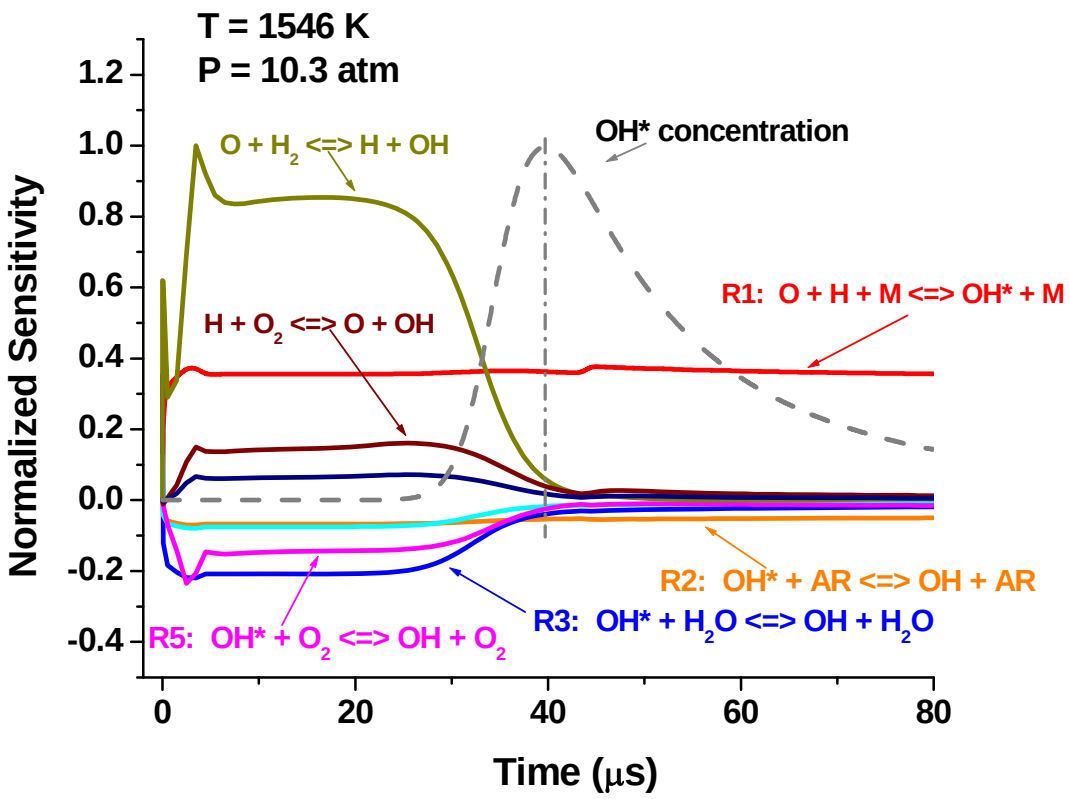

Figure 10. A local sensitivity analysis with respect to OH* shows the most important reaction at the peak is R1: O + H + M = OH* + M at 1546K, 10.3 atm. For clarity, only the most influential reactions are shown.

The correct reaction rate of R1 could then be found at each measured temperature and pressure by matching the model predicted peak of OH* to the experimentally obtained peak. An iterative procedure was used to set the reaction rate of R1 to a constant value for each experimental condition until peak values of the data and model aligned within

1%. Resulting reaction rates are given in Table 3. An example of this procedure for the test condition of 1941 K, 10.6 atm is seen in Figure 11. Note in Figure 11 that the model was shifted to align the profile peaks for clarity (since the OH* kinetics have no affect on the overall timing of the H_2-O_2 reaction, which is dominated by the main H_2 oxidation mechanism). In order to analyze the pressure dependence in the typical Lindemann form [44], the reaction rate used to calibrate the peak was actually the bimolecular reaction rate (in units of cm^3/mol-s) for R1 written as

$$O + H = OH^*$$

as opposed to the termolecular reaction rate, k (in units of cm^6/mol^2-s) for R1 written as $O + H + M = OH^* + M$.

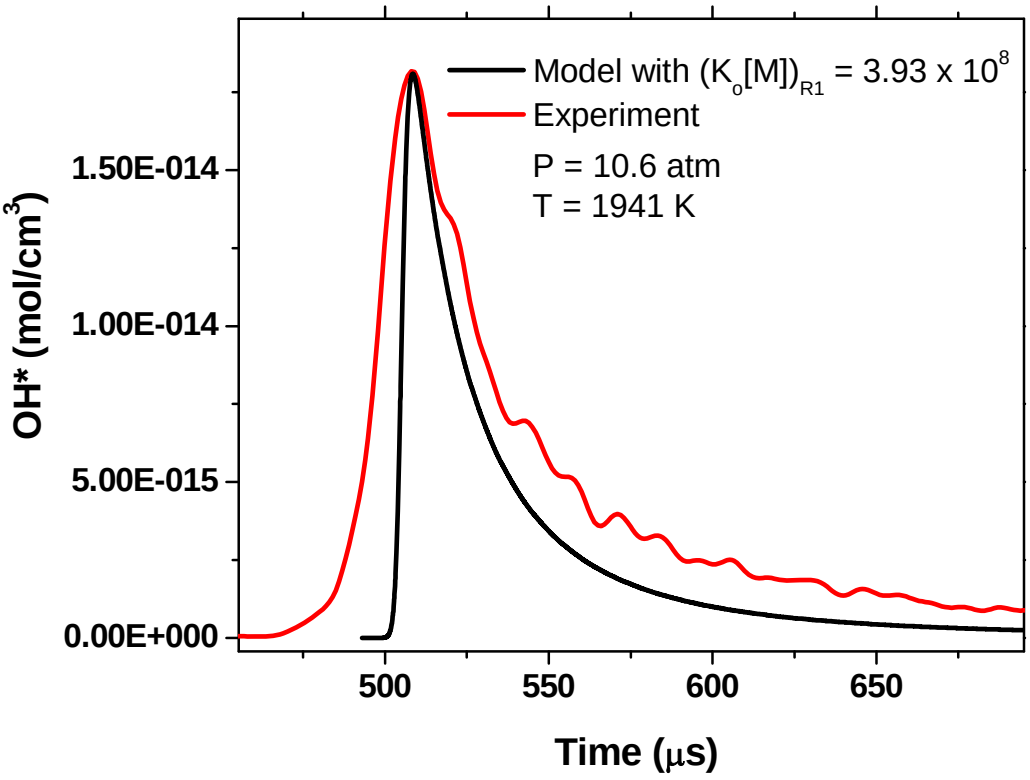

Figure 11. The constant reaction rate of R1 was iteratively changed until peak concentrations agreed within 1% for all experimental test cases as seen here for T = 1941 K and 10.6 atm.

Table 3. Constant value bimolecular reaction rates for each experimental condition that yield peak concentration of OH* within 1% of experimentally obtained peaks.

Pressure (atm)	Temperature (K)	K (cm^3/mol-s)
10.3	1316	4.880E+08
10.3	1546	3.620E+08
10.3	1781	4.000E+08
10.3	1941	3.930E+08
10.3	2121	5.470E+08
10.3	2234	7.300E+08
14	1387	6.485E+08
14	1535	4.650E+08
14	1561	5.070E+08
14	1729	5.000E+08
14	1914	5.690E+08
14	2163	8.050E+08

Once the rate coefficients were obtained for the entire range of experimental conditions, modified Arrhenius fits of the rates were performed at 10.3 and 14 atm, yielding equations that give the reaction rates as a function of temperature. Miller and Lutz [58] developed a generalized method for including the pressure dependence of a reaction rate based on direct interpolation of reaction rates specified at individual pressures. With different rate parameters given for discrete pressures within the pressure range of interest, the actual reaction rate is determined through logarithmic interpolation

of the specified rate constants. If the desired pressure is within 1% of one of the pressures provided, then that rate will be used. If the desired pressure is between the pressures provided, then the rate will be determined through linear interpolation of the natural log of the reaction, ln(k) as a function of the natural log of pressure, ln(P) as shown below for some P between P_i and P_{i+1}:

$$\ln k = \ln k_i + (\ln k_{i+1} - \ln k_i) \times \frac{\ln P - \ln P_i}{\ln P_{i+1} - \ln P_i}$$

The new pressure dependent bimolecular reaction rate for R1 is shown in Table 4.

Table 4. Pressure-dependent bimolecular rate coefficients of R1. Rate coefficients are expressed as $k[M] = AT^n exp(-E/RT)$ with units of cal, mol, cm, and s.

#	Reaction	Pressure (atm)	A	n	E (kcal)
1	O + H = OH*	1.3	2.28×10^{9}	0.0	9829.9
		10.3	$4.56 \times 10^{-46(\pm 9)}$	14.8 (±2.5)	-47.66(±8.4)
		14	$6.41 \times 10^{-52(\pm 9)}$	16.4(±2.3)	-53.97(±7.7)

The reaction rates as a function of inverse temperature increase with increasing pressure as seen in Figure 12. Over the range of conditions in this study, k varies by an order of magnitude.

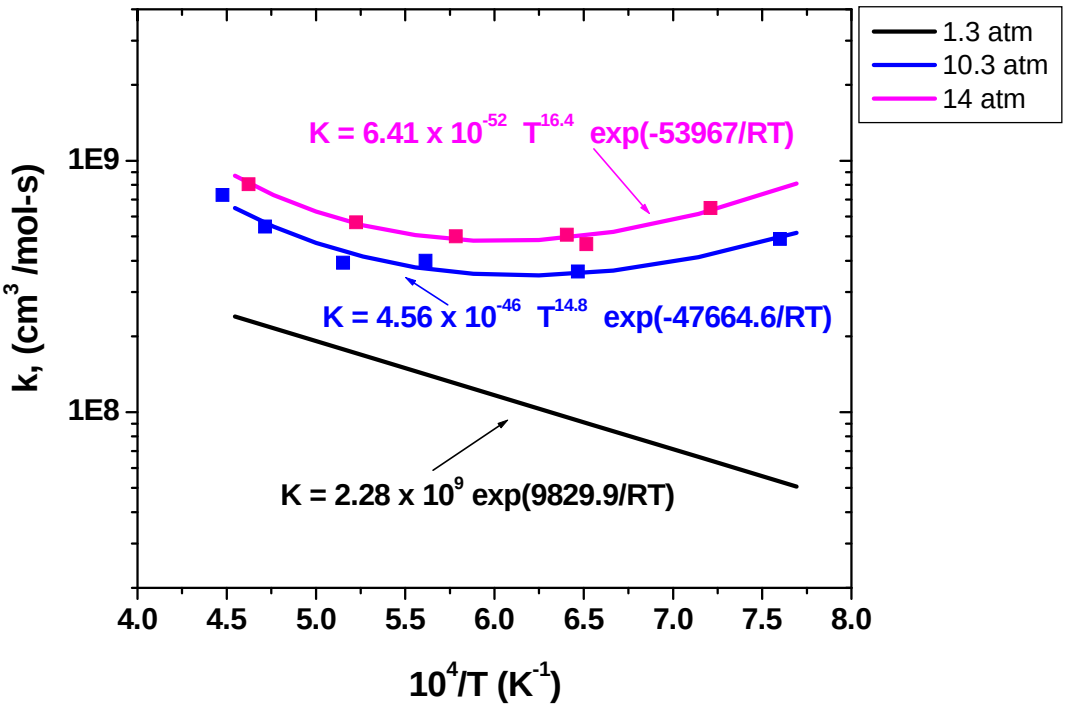

Figure 12. The reaction rate for R1 as a function of temperature increases with increasing pressure. Lines represent Arrhenius fits, data symbols represent experimentally obtained reaction rate values given in Table 3.

The new pressure-dependent reaction rate was added to the mechanism and compared to the experimental data, Figure 13. The model now accurately predicts the peak concentration of OH* at higher pressures. The reaction rate increases with increasing pressure. This trend is shown in Figure 14a-c for three different temperatures, where the solid symbols represent the reaction rate at the conditions of this study, and the open symbol represents the interpolated value of k[M] at 5 atm.

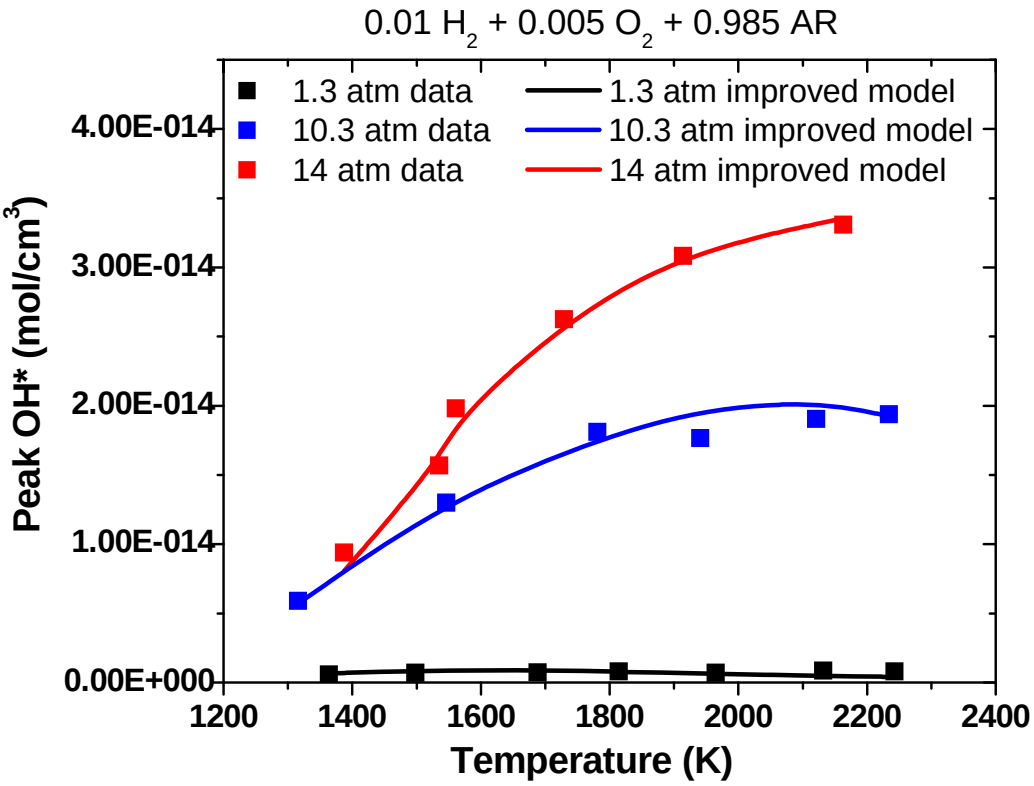

Figure 13. The improved pressure-dependent reaction rate greatly improves the agreement between the model (lines) and the data (points) at elevated pressure.

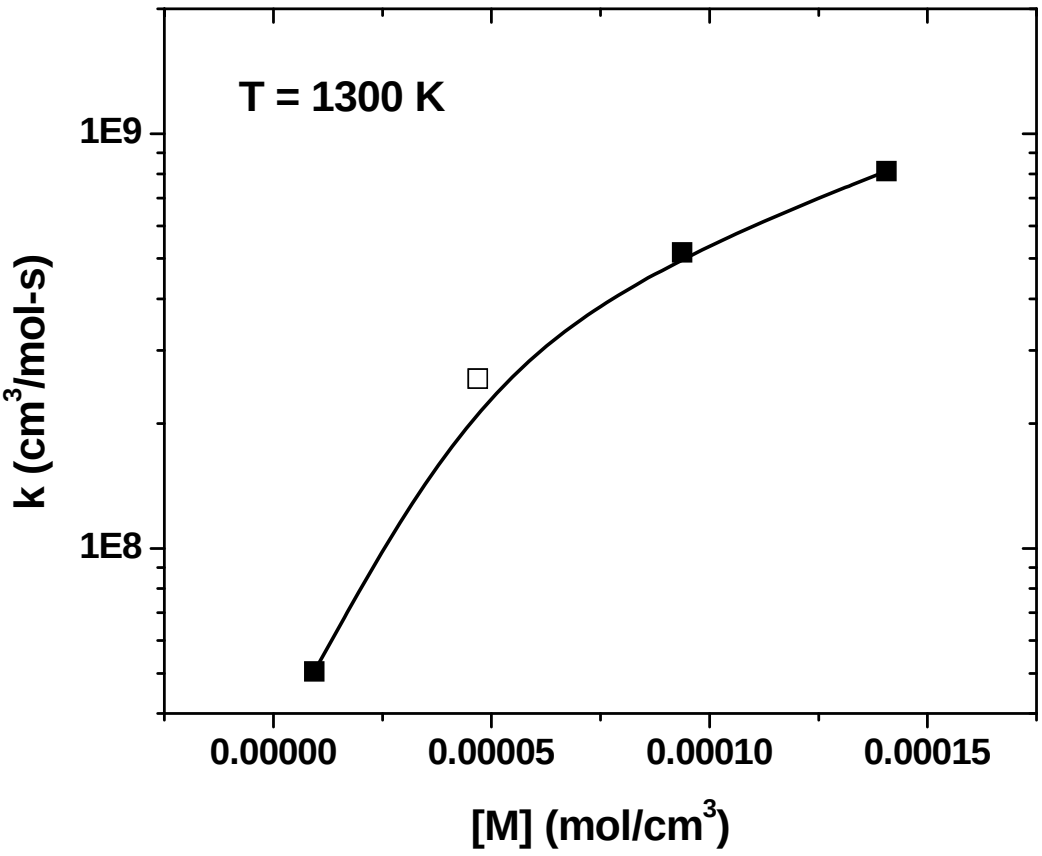

(a) T = 1300 K

Figure 14. The pressure-dependent reaction rate shown on a typical Lindemann-style plot at three different temperatures. Closed squares represent reaction rates developed in this work, open squares represent logarithmic interpolation at 5 atm, and lines are best fit curves of the data.

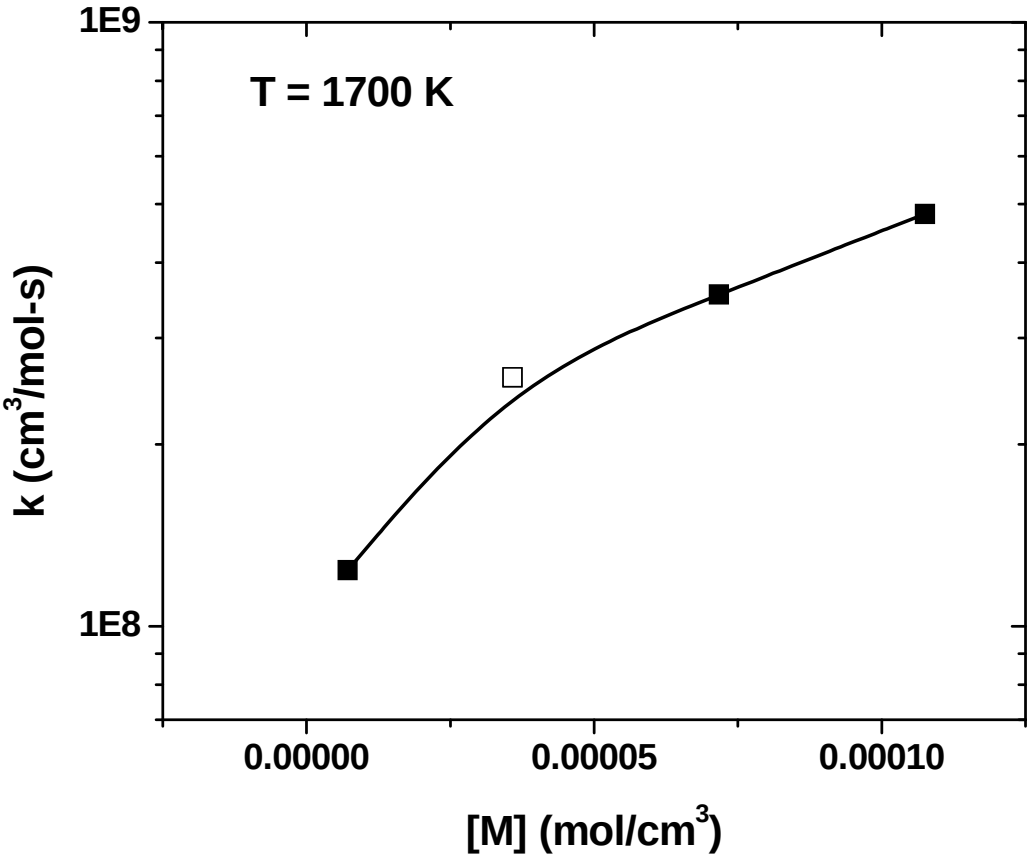

(b) T = 1700 K

Figure 14 continued

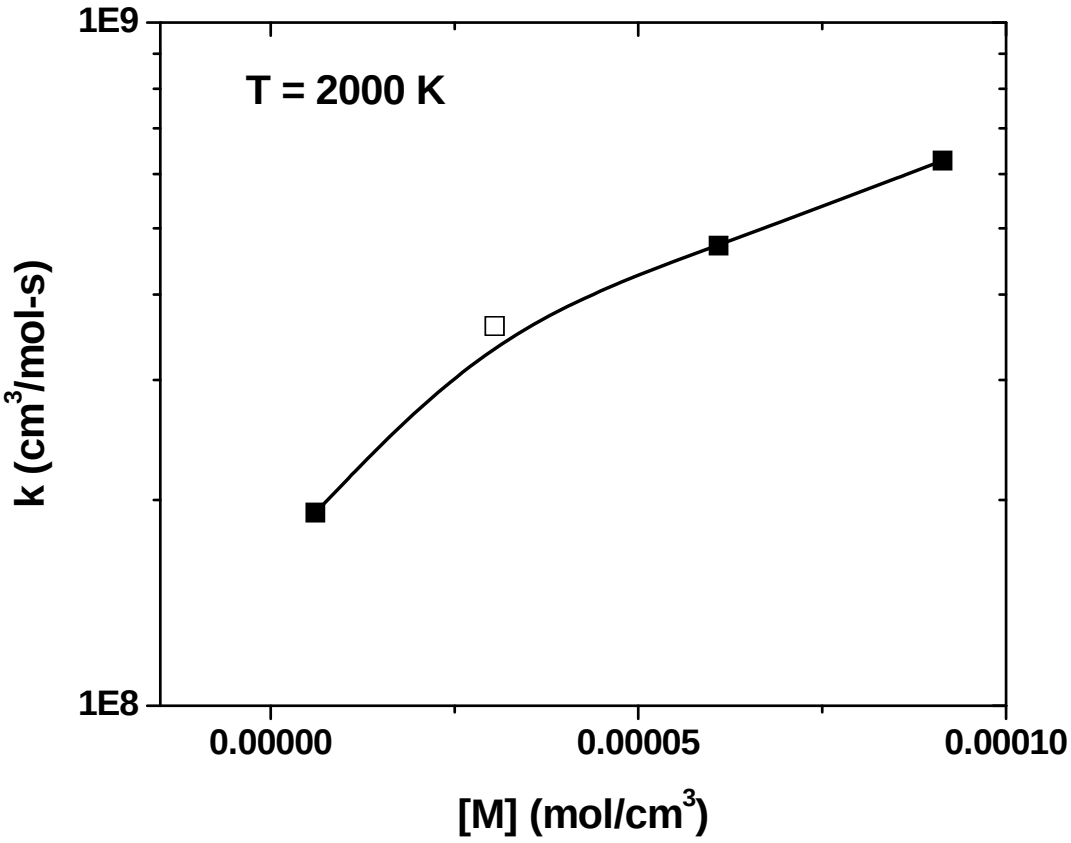

(c) T = 2000 K

Figure 14 continued

CHAPTER VI

CONCLUSIONS AND RECOMMENDATIONS

The measurement of chemiluminescence from OH* provides an inexpensive and nonintrusive diagnostic ideal for use in many practical combustion systems. The key to utilizing this type of measurement is to have an accurate kinetics model that relates the qualitative, measured emission to the absolute concentration. It was determined that while the kinetics model is accurate at atmospheric conditions, it significantly over predicts the OH* concentration at higher pressures, thus making the original OH* kinetics model invalid at the elevated pressure of interest to most engine applications. Thus, the pressure dependence of the rate of O + H = OH* was determined and validated up to 15 atm. Constant optical settings were maintained through a set of shock-tube experiments at 3 different pressure regimes (1, 10, and 15 atm). A calibration curve was developed from low-pressure experiments, where the kinetics are relatively well known, and extrapolated to the high-pressure region of interest. The derived rate expression in bimolecular form (with units of cm^3/mol-s) is as follows.

P = 1.3 atm $$k = 2.28 \times 10^{9} \exp\left(\frac{-9829.9}{RT}\right)$$

P = 10.3 atm $$k = 4.56 \times 10^{-46} T^{14.8} \exp\left(\frac{47664.6}{RT}\right)$$

P = 14 atm $$k = 6.41 \times 10^{-52} T^{16.4} \exp\left(\frac{53967.1}{RT}\right)$$

This new rate for R1 improves the existing kinetics model at elevated pressure and is able to reproduce the entire range of data collected. This new model enables the

use of OH chemiluminescence as a quantitative emission diagnostic in practical combustion applications.

At the conclusion of this work, it is the author's recommendation that further experiments be performed at pressures above 15 atm; between 1 and 5 atm; and below 1 atm to obtain an even better measurement of the pressure dependence of the title reaction. Due to the successful calibration developed herein to relate OH* emission to absolute OH* concentration, experiments can now be performed to extend the calibration curve above 700 mV (ie higher pressures). As seen in Figure 14 by the leveling off of k at the higher pressures, the high-pressure limit may be reached and thus modeled in the traditional Linemann or Troe methods. Similarly, pressure below 1 atm will ensure that the low-pressure limit is also quantified.

REFERENCES

[1] Higgins, B.; McQuay, M. Q.; Lacas, F.; Rolon, J. C.; Darabiha, N.; and Candel, S. "Systematic Measurements of OH-Chemiluminescence for Fuel-Lean, High-Pressure, Pre-Mixed Laminar Flames," *Fuel,* Vol. 80, No. 1, 2001, pp. 67–74.

[2] Docquier, N.; Belhalfaoui, S.; Lacas, F.; Darabiha, N.; and Rolon, C. "Experimental and Numerical Study of Chemiluminescence in Methane/Air High-Pressure Flames for Active Control Applications," *Proceedings of the Combustion Institute*, Vol. 28, 2000, pp. 1765-174.

[3] Hardalupas, Y.,; and Orain, M., "Local Measurements of the Time-Dependent Heat Release Rate and Equivalence Ratio using Chemiluminescent Emission from a Flame," *Combustion and Flame*, Vol. 139, No. 3, 2004, pp.188-207.

[4] Muruganandam, T. M.; Kim, B. H.; Morrell, M. R.; Nori, V.; Patel, M.; Romig, B. W.; and Seitzman, J. M. "Optical Equivalence Ratio Sensors for Gas Turbine Combustors," *Proceedings of the Combustion Institute*, Vol. 30, 2005, pp. 1601–1609.

[5] Nori, V.; and Seitzman, J. "Evaluation of Chemiluminescence as a Combustion Diagnostic under Varying Operating Conditions," AIAA paper 2008-953, 2008.

[6] Kojima, J.; Ikeda, Y.; and Nakajima, T. "Basic Aspects of OH(A), CH(A), and C_2(d) Chemiluminescence in the Reaction Zone of Laminar Methane-Air Flames," *Combustion and Flame,* Vol. 140, 2005, pp. 34-45.

[7] Locke, R. J.; and Ockunzzi, K. A.. "OH Imaging in a Lean Burning High-Pressure Combustor," *AIAA Journal Technical Note*, Vol. 34, No. 3, 1996, pp. 622-624.

[8] Roby, R. J.; Hamer, A. J.; Johnsson, E. L.; Tilstra, S. A.; Burt, T. J. "Improved Method for Flame Detection in Combustion Turbines," *Journal of Engineering for Gas Turbines and Power*, Vol. 117, 1995, pp. 332-340.

[9] Edwards, D. H.; Davies, G. T.; and Phillips, D. E. "The Measurement of Temperature in Shock-Heated Gases from the Relative Intensities of the OH Ultraviolet Bands," *Journal of Physics D: Applied Physics,* Vol. 7, 1974, pp. 2562-2575.

[10] Gaydon, A. G. *The Spectroscopy of Flames*, Chapman and Hall, London, 1957.

[11] Charton, M.; and Gaydon, A. G. "Excitation of Spectra of OH in Hydrogen Flames and Its Relation to Excess Concentrations of Free Atoms," *Proceedings of the Royal Society of London A, Mathematical and Physical Sciences*, Vol. 245, 1958, pp. 84–92.

[12] Kaskan, W. E. "Abnormal Excitation of OH in $H_2/O_2/N_2$ Flames," *The Journal of Chemical Physics*, Vol. 31, 1959, pp. 944–956.

[13] Zeegers, P. J. TH.; and Alkemade, C. TH. J. "Chemiluminescence of OH Radicals and K Atoms By Radical Recombination in Flames," *Proceedings of the Combustion Institute*, Vol. 10, 1965, pp. 33–40.

[14] Ticktin, S.; Spindler, G.; and Schiff, H. I. "Production of Excited OH($A^2\Sigma^+$) Molecules by the Association of Ground-State Oxygen and Hydrogen Atoms," *Discussions of the Faraday Society*, Vol. 44, 1967, pp. 218–240.

[15] Hollander, Tj. “Photometric Measurements on the Deviations from the Equilibrium State in Flames,” *AIAA Journal*, Vol. 6, No. 3, 1968, pp. 385–393.

[16] Davis, M. G.; McGregor, W. K.; and Mason, A. A. “OH Chemiluminescent Radiation from Lean Hydrogen-Oxygen Flames,” *The Journal of Chemical Physics*, Vol. 61, No. 4, 1974, pp. 1352–1356.

[17] Smith, G. P.; Luque, J.; Park, C.; Jeffries, J. B.; and Crosley, D. R. "Low Pressure Flame Determinations of Rate Constants for OH(A) and CH(A) Chemiluminescence," *Combustion and Flame*, Vol. 131, No. 1 – 2, 2002, pp. 59-69.

[18] Smith, G. P.; Park, C.; and Luque, J. “A Note on Chemiluminescence in Low-Pressure Hydrogen and Methane-Nitrous Oxide Flames,” *Combustion and Flame*, Vol. 140, 2005, pp. 385–389.

[19] Walsh, K. T.; Long, M. B.; Tanoff, M. A.; and Smooke, M. D. “Experimental and Computational Study of CH, CH*, and OH* in an Axisymmetric Laminar Diffusion Flame,” *Twenty-Seventh Symposium (International) on Combustion/The Combustion Institute,* 1998, pp. 615-623.

[20] Luque, J.; Jeffries, J. B.; Smith, G. P.; Crosley, D. R.; Walsh, K. T.; Long, M. B.; and Smooke, M. D. “CH(A-X) and OH(A-X) Optical Emission in an Axisymmetric Laminar Diffusion Flame,” *Combustion and Flame,* Vol. 122, 2000, pp. 172-175.

[21] Haber, L. C.; and Vandsburger, U. “A Global Reaction Model for OH* Chemiluminescence Applied to a Laminar Flat-Flame Burner,” *Combustion Science and Technology,* Vol 175, No. 10, 2003, pp. 1859-1891.

[22] Dandy, D. S.; and Vosen, S. R. "Numerical and Experimental Studies of Hydroxyl Radical Chemiluminescence in Methane-Air Flames," *Combustion Science and Technology,* Vol. 82, 1992, pp. 131- 148.

[23] Belles, F. E.; and Lauver, M. R. "Origin of OH Chemiluminescence during the Induction Period of the H_2-O_2 Reaction Behind Shock Waves," *The Journal of Chemical Physics*, Vol. 40, No. 2, 1964, pp. 415–422.

[24] Gutman, D.; Lutz, R. W.; Jacobs, N. F.; Hardwidge, E. A.; and Schott, G. L. "Shock-Tube Study of OH Chemiluminescence in the Hydrogen-Oxygen Reaction," *The Journal of Chemical Physics*, Vol. 48, No. 12, 1968, pp. 5689–5694.

[25] Gardiner, W. C. Jr.; Morinaga, K.; Ripley, D. L.; and Takeyama, T. "Shock-Tube Study of OH($^2\Sigma - {}^2\Pi$) Luminescence," *The Physics of Fluids Supplement*, Vol. 1, 1969, pp. 120–124.

[26] Hidaka, Y.; Takahashi, S.; Kawano, H.; Suga, M.; and Gardiner, W. C. Jr. "Shock Tube Measurement of the Rate Constant for Excited OH($A^2\Sigma^+$) Formation in the Hydrogen-Oxygen Reaction," *The Journal of Physical Chemistry*, Vol. 86, 1982, pp. 1429–1433.

[27] Koike, T.; and Morinaga, K. "Further Studies of the Rate Constant for Chemical Excitation of OH in Shock Waves," *Bulletin of the Chemical Society of Japan*, Vol. 55, No. 1, 1982, pp. 52–54.

[28] Paul, P. H.; Durant, J. L. Jr.; Gray, J. A.; and Furlanetto, M. R. "Collisional Electronic Quenching of OH $A^2\Sigma$ (v'=0) Measured at High Temperature in a Shock Tube," *The Journal of Chemical Physics*, Vol. 102, No. 21, 1995, pp. 8378–8384.

[29] Petersen, E. L.; Kalitan, D. M.; and Rickard, M. J. A. "Calibration and Chemical Kinetics Modeling of an OH Chemiluminescence Diagnostics," AIAA paper 2003-4493, 2003.

[30] Hall, J. M.; Petersen, E. L. "An Optimized Kinetics Model for OH Chemiluminescence at High Temperatures and Atmospheric Pressures," *International Journal of Chemical Kinetics,* Vol. 38, Issue 12, 2006, pp. 714-724.

[31] Kathrotia, T.; Riedel, U.; Hartmann, M.; Bozkurt, M.; Fikri, M.; and Schulz, C. "Study of the H+O+M reaction forming OH*: Kinetics of OH* Chemiluminescence in Hydrogen Combustion Systems," *Combustion and Flame,* in press.

[32] Carl, S. A.; Van Poppel, M.; and Peeters, J. "Identification of the CH + O_2 → OH(A) + CO Reaction as the Source of OH(A—X) Chemiluminescence in C_2H_2/O/H/O_2 Atomic Flames and Determination of Its Absolute Rate Constant Over the Range T = 296 to 511 K," *Journal of Physical Chemistry A*, Vol. 107, 2003, pp. 11001–11007.

[33] Grebe, J.; and Homann, K. H., "Kinetics of the Species OH($A^2\Sigma^+$), OH($X^2\Pi$) and CH($X^2\Pi$) in the System C_2H_2/O/H," *Berichte der Bunsen-Gesellschaft für Physikalische Chemie*, Vol. 86, 1982, pp. 581–587.

[34] Porter, R. P.; Clark, A. H.; Kaskan, W. E.; and Browne, W. E. "A Study of Hydrocarbon Flames," *Proceedings of the Combustion Institute*, Vol. 11, 1967, pp. 907-917.

[35] Marques, C. S. T; Benvenutti, L.H.; and Bertran, C.A. "Kinetic Modeling for Chemiluminescent Radicals in Acetylene Combustion," *Journal of the Brazilian Chemical Society,* Vol. 17, No. 2, 2006, pp.302-315.

[36] Skrebkov, O.V.; Karkach, S. P.; Vasil'ev, V. M.; Smirnov, A. L. "Hydrogen-Oxygen Reactions Behind Shock Waves Assisted by OH($^2\Sigma^+$) Formation," *Chemical Physics Letters,* Vol. 375, 2003, pp. 413-418.

[37] Tamura, M.; Berg, P. A.; Harrington, J. E.; Luque, J.; Jeffries, J. B.; Smith, G. P.; Crosley, D. R. "Collisional Quenching of CH(A), OH(A), and NO(A) in Low Pressure Hydrocarbon Flames," *Combustion and Flame*, Vol. 114, 1998, pp. 502–514.

[38] German, K. R. "Direct Measurement of the Radiative Lifetimes of the $A^2\Sigma^+$ (V' = 0) States of OH and OD," *The Journal of Chemical Physics,* Vol. 62, No. 7, 1975, pp. 2584-2587.

[39] Fairchild, P. W.; Smith, G. P.; Crosley, D. R. "Collisional Quenching of A2Σ+ OH at Elevated Temperatures," *The Journal of Chemical Physics*, Vol. 79, No. 4, 1983, pp. 1795–1807.

[40] Esposti, A. D.; Werner, H. J. "Ab Initio Calculation of the OH($X^2\Pi$,$A^2\Sigma^{+)}$+Ar Potential Energy Surfaces and Quantum Scattering Studies of Rotational Energy Transfer in the OH($A^2\Sigma^+$) State," *The Journal of Chemical Physics*, Vol. 93, No. 5, 1990, pp. 3351–3366.

[41] Jörg, A.; Meier, U.; Kohse-Höinghaus, K. "Rotational Energy Transfer in OH($A^2\Sigma^+$, ν'=0): A Method for the Direct Determination of State-to-State Transfer

Coefficients," *The Journal of Chemical Physics*, Vol. 93, No. 9, 1990, pp. 6453–6462.

[42] Petersen, E. L. "Interpreting Endwall and Sidewall Measurements in Shock-Tube Studies," *Combustion Science and Technology,* Vol. 181, 2009, pp. 1123-1144.

[43] Gilbert, R. G.; and Smith, S. C. Theory of Unimolecular and Recombination Reactions; Blackwell: Oxford, 1990.

[44] Lindemann, F. "Discussion on The Radiation Theory of Chemical Action," *Transactions of the Faraday Society,* Vol 17, 1922, pp. 598 – 606.

[45] Aul, C. J.; de Vries, J.; and Petersen, E. L., "New Shock-Tube Facility for Studies in Chemical Kinetics at Engine Conditions," *Eastern States Fall Technical Meeting of the Combustion Institute*, Oct. 21-24, 2007, Charlottesville, VA.

[46] Rickard, M. J. A.; Petersen, E. L., "Optimization of a Photomultiplier Tube Detector for the Measurement of Low Light Levels in High-speed Reacting Flows," Aerospace Corporation, Internal Report. Los Angeles, Ca.

[47] Kee, R. J.; Rupley, F. M.; Miller, J. A.; Coltrin, M. E.; Grcar, J. F.; Meeks, E.; Moffat, H. K.; Lutz, A. E.; Dixon-Lewis, G.; Smooke, M. D.; Warnatz, J.; Evans, G. H.; Larson, R. S.; Mitchell, R. E.; Petzold, L. R.; Reynolds, W. C.; Caracotsios, M.; Stewart, W. E.; Glarborg, P.; Wang, C.; and Adigun, O. Chemkin Collection, Release 4.1.1, Reaction Design, Inc., San Diego, CA, 2007.

[48] Smith, G. P.; Golden, D. M.; Frenklach, M.; Moriarty, N. W.; Eiteneer, B.; Goldenberg, M.; Bowman, C. T.; Hanson, R. K.; Song, S.; Gardiner, W. C. Jr.; Lissianski, V. V.; and Qin, Z. GRI-Mech 3. 0, http://www.me.berkeley.edu/gri-mech/

[49] Ó Conaire, M.; Curran, H. J.; Simmie, J. M.; Pitz, W. J.; Westbrook, C. K. "A Comprehensive Modeling Study of Hydrogen Oxidation," *International Journal of Chemical Kinetics,* Vol. 36, No. 11, 2004, pp. 603– 622.

[50] Healy, D.; Curran, H. J.; Simmie, J. M.; Kalitan, D. M.; Zinner, C. M.; Barrett, A. B.; Petersen, E. L.; and Bourque, G. "Methane/Ethane/Propane Mixture Oxidation at High Pressures and at High, Intermediate and Low Temperatures," *Combustion and Flame*, Vol. 155, No. 3, 2008, pp. 441–448.

[51] Healy, D.; Curran, H. J.; Dooley, S.; Simmie, J. M.; Kalitan, D. M.; Petersen, E. L.; and Bourque, G. " Methane/Propane Mixture Oxidation at High Pressures and at High, Intermediate and Low Temperatures," *Combustion and Flame*, Vol. 155, No. 3, 2008, pp. 451–461.

[52] Petersen, E. L.; Hall, J. M.; Smith, S. D.; de Vries, J.; Amadio, A. R.; and Crofton, M. W. "Ignition of Lean Methane-Based Fuel Blends at Gas Turine Pressures," *Journal of Engineering for Gas Turbines and Power,* Vol. 129, 2007, pp. 937-944.

[53] Curran, H. J.; Healy, D.; Donato, N.; Aul, C.; Petersen, E. L.; Zinner, C.; Bourque, G. "n-Butane: Ignition Delay Measurements at High Pressure and Detailed Chemical Kinetic Simulations," *Combustion and Flame,* in press.

[54] Curran, H. J.; Healy, D.; Donato, N.; Aul, C.; Zinner, C.; Petersen, E. L.; Bourque, G. "iso-Butane: Ignition Delay Measurements at High Pressure and Detailed Chemical Kinetic Simulations," *Combustion and Flame,* in press.

[55] Donato, N. S.; Aul, C.; Petersen, E.; Zinner, C.; Healy, D.; Curran, H. J.; Bourque, G. "Ignition and Oxidation of 50/50 n-Butane/iso-Butane Blends," *Journal of Engineering for Gas Turbines and Power*, 2010, in press.

[56] "Third Millennium Ideal Gas and Condensed Phase Thermochemical Database for Combustion with updates from Active Thermochemical Tables" ANL-05/20 and TAE 960 Technion-IIT, Aerospace Engineering, and Argonne National Laboratory, Chemistry Division, Argonne, IL, September 2005.

[57] Petersen, E. L.; Rickard, M. J. A.; Crofton, M.W.; Abbey, E. D.; Traum, M. J.; and Kalitan, D. M., "A Facility for Gas- and Condensed-Phase Measurements Behind Shock Waves," *Measurement Science and Technology*, Vol. 16, No. 9, 2005, pp. 1716–1729.

[58] Kee, R. J.; Rupley, F. M.; Miller, J. A.; Coltrin, M. E.; Grcar, J. F.; Meeks, E.; Moffat, H. K.; Lutz, A. E.; Dixon-Lewis, G.; Smooke, M. D.; Warnatz, J.; Evans, G. H.; Larson, R. S.; Mitchell, R. E.; Petzold, L. R.; Reynolds, W. C.; Caracotsios, M.; Stewart, W. E.; Glarborg, P.; Wang, C.; and Adigun, O. "Theory Manual," Chemkin Collection, Release 4.1.1, Reaction Design, Inc., San Diego, CA, 2007.

APPENDIX A

SPECIES IN THE DETAILED MODEL

ELEMENTS CONSIDERED	ATOMIC WEIGHT
1. O	15.9994
2. H	1.00797
3. C	12.0112
4. N	14.0067
5. AR	39.9480

SPECIES CONSIDERED	MOLECULAR WEIGHT	TEMPERATURE LOW	TEMPERATURE HIGH	ELEMENT COUNT O	H	C	N	AR
1. H2	2.0159E+00	200	3500	0	2	0	0	0
2. H	1.0080E+00	200	3500	0	1	0	0	0
3. O	1.5999E+01	200	3500	1	0	0	0	0
4. O2	3.1999E+01	200	3500	2	0	0	0	0
5. OH	1.7007E+01	200	3500	1	1	0	0	0
6. H2O	1.8015E+01	200	3500	1	2	0	0	0
7. HO2	3.3007E+01	200	3500	2	1	0	0	0
8. H2O2	3.4015E+01	200	3500	2	2	0	0	0
9. C	1.2011E+01	200	3500	0	0	1	0	0
10. CH	1.3019E+01	200	3500	0	1	1	0	0
11. CH2	1.4027E+01	200	3500	0	2	1	0	0
12. CH2(S)	1.4027E+01	200	3500	0	2	1	0	0
13. CH3	1.5035E+01	200	3500	0	3	1	0	0
14. CH4	1.6043E+01	200	3500	0	4	1	0	0
15. CO	2.8011E+01	200	3500	1	0	1	0	0
16. CO2	4.4010E+01	200	3500	2	0	1	0	0
17. HCO	2.9019E+01	200	3500	1	1	1	0	0
18. CH2O	3.0026E+01	200	3500	1	2	1	0	0
19. CH2OH	3.1034E+01	200	3500	1	3	1	0	0

SPECIES CONSIDERED	MOLECULAR WEIGHT	TEMPERATURE LOW	TEMPERATURE HIGH	ELEMENT O	ELEMENT H	ELEMENT C	COUNT N	COUNT AR
20. CH3O	3.1034E+01	300	3000	1	3	1	0	0
21. CH3OH	3.2042E+01	200	3500	1	4	1	0	0
22. C2H	2.5030E+01	200	3500	0	1	2	0	0
23. C2H2	2.6038E+01	200	3500	0	2	2	0	0
24. C2H3	2.7046E+01	200	3500	0	3	2	0	0
25. C2H4	2.8054E+01	200	3500	0	4	2	0	0
26. C2H5	2.9062E+01	200	3500	0	5	2	0	0
27. C2H6	3.0070E+01	200	3500	0	6	2	0	0
28. HCCO	4.1030E+01	300	4000	1	1	2	0	0
29. CH2CO	4.2038E+01	200	3500	1	2	2	0	0
30. HCCOH	4.2038E+01	300	5000	1	2	2	0	0
31. N	1.4007E+01	200	6000	0	0	0	1	0
32. NH	1.5015E+01	200	6000	0	1	0	1	0
33. NH2	1.6023E+01	200	6000	0	2	0	1	0
34. NH3	1.7031E+01	200	6000	0	3	0	1	0
35. NNH	2.9021E+01	200	6000	0	1	0	2	0
36. NO	3.0006E+01	200	6000	1	0	0	1	0
37. NO2	4.6005E+01	200	6000	2	0	0	1	0
38. N2O	4.4013E+01	200	6000	1	0	0	2	0
39. HNO	3.1014E+01	200	6000	1	1	0	1	0
40. CN	2.6018E+01	200	6000	0	0	1	1	0
41. HCN	2.7026E+01	200	6000	0	1	1	0	0
42. H2CN	2.8034E+01	300	4000	0	2	1	1	0
43. HCNN	4.1033E+01	300	5000	0	1	1	2	0
44. HCNO	4.3025E+01	300	5000	1	1	1	1	0
45. HOCN	4.3025E+01	300	5000	1	1	1	1	0

SPECIES CONSIDERED	MOLECULAR WEIGHT	TEMPERATURE LOW	TEMPERATURE HIGH	ELEMENT O	ELEMENT H	ELEMENT C	COUNT N	COUNT AR
46. HNCO	4.3025E+01	300	5000	1	1	1	1	0
47. NCO	4.2017E+01	200	6000	1	0	1	1	0
48. N2	2.8013E+01	300	5000	0	0	0	2	0
49. AR	3.9948E+01	300	5000	0	0	0	0	1
50. C3H7	4.3089E+01	300	5000	0	7	3	0	0
51. C3H8	4.4097E+01	300	5000	0	8	3	0	0
52. CH2CHO	4.3046E+01	300	5000	1	3	2	0	0
53. CH3CHO	4.4054E+01	200	6000	1	4	2	0	0
54. OH(A)	1.7007E+01	300	5000	1	1	0	0	0
55. CH(A)	1.3019E+01	300	5000	0	1	1	0	0
56. C2	2.4022E+01	300	5000	0	0	2	0	0

APPENDIX B

REACTIONS IN THE DETAILED MODEL

	REACTIONS CONSIDERED			(k = A T**b exp(-E/RT)) A	b	E
1.	2O+M<=>O2+M			1.20E+17	-1.0	0.0
	H2	Enhanced by	2.400E+00			
	H2O	Enhanced by	1.540E+01			
	CH4	Enhanced by	2.000E+00			
	CO	Enhanced by	1.750E+00			
	CO2	Enhanced by	3.600E+00			
	C2H6	Enhanced by	3.000E+00			
	AR	Enhanced by	8.300E-01			
2.	O+H+M<=>OH+M			5.00E+17	-1.0	0.0
	H2	Enhanced by	2.000E+00			
	H2O	Enhanced by	6.000E+00			
	CH4	Enhanced by	2.000E+00			
	CO	Enhanced by	1.500E+00			
	CO2	Enhanced by	2.000E+00			
	C2H6	Enhanced by	3.000E+00			
	AR	Enhanced by	7.000E-01			
3.	O+H+M<=>OH(A)+M			3.10E+14	0.0	10000.0
	H2	Enhanced by	2.000E+00			
	H2O	Enhanced by	6.000E+00			
	CH4	Enhanced by	2.000E+00			
	CO	Enhanced by	1.500E+00			
	CO2	Enhanced by	2.000E+00			
	C2H6	Enhanced by	3.000E+00			
	AR	Enhanced by	7.000E-01			
4.	CH+O2<=>OH(A)+CO			3.24E+14	-0.4	4150.0
5.	OH(A)+AR<=>OH+AR			2.17E+10	0.5	2060.0
6.	OH(A)+H2O<=>OH+H2O			5.92E+12	0.5	-861.0
7.	OH(A)+CO2<=>OH+CO2			2.75E+12	0.5	-968.0
8.	OH(A)+CO<=>OH+CO			3.23E+12	0.5	-787.0
9.	OH(A)+H2<=>OH+H2			2.95E+12	0.5	-444.0
10.	OH(A)+O2<=>OH+O2			2.10E+12	0.5	-482.0
11.	OH(A)+OH<=>OH+OH			1.50E+12	0.5	0.0
12.	OH(A)+H<=>OH+H			1.50E+12	0.5	0.0
13.	OH(A)+O<=>OH+O			1.50E+12	0.5	0.0
14.	OH(A)+CH4<=>OH+CH4			3.36E+12	0.5	-635.0
15.	OH(A)<=>OH			1.40E+06	0.0	0.0
16.	OH(A)+N2<=>OH+N2			1.08E+11	0.5	-1238.0
17.	C2+OH<=>CO+CH(A)			2.00E+14	0.0	0.0
18.	C2H+O<=>CO+CH(A)			5.20E+11	0.0	2600.0
19.	C+H+M<=>CH(A)+M			3.63E+13	0.0	0.0
20.	CH(A)=>CH			1.86E+06	0.0	0.0
21.	CH(A)+N2=>CH+N2			3.03E+02	3.4	-381.0
22.	CH(A)+AR=>CH+AR			4.00E+10	0.5	0.0
23.	CH(A)+O2=>CH+O2			2.48E+06	2.1	-1720.0
24.	CH(A)+H2O=>CH+H2O			5.30E+13	0.0	0.0
25.	CH(A)+H2=>CH+H2			1.47E+14	0.0	1361.0

```
26. CH(A)+CO2=>CH+CO2                             2.41E-01    4.3    -1694.0
27. CH(A)+CO=>CH+CO                               2.44E+12    0.5        0.0
28. CH(A)+CH4=>CH+CH4                             1.73E+13    0.0      167.0
29. C2+H2<=>C2H+H                                 4.00E+05    2.4     1000.0
30. CH+CH<=>C2+H2                                 5.00E+12    0.0        0.0
31. C+C+M<=>C2+M                                  3.00E+14    0.0    -1000.0
32. C+CH<=>C2+H                                   5.00E+13    0.0        0.0
33. O+C2<=>C+CO                                   5.00E+13    0.0        0.0
34. C2+O2<=>CO+CO                                 9.00E+12    0.0      980.0
35. O+H2<=>H+OH                                   3.87E+04    2.7     6260.0
36. O+HO2<=>OH+O2                                 2.00E+13    0.0        0.0
37. O+H2O2<=>OH+HO2                               9.63E+06    2.0     4000.0
38. O+CH<=>H+CO                                   5.70E+13    0.0        0.0
39. O+CH2<=>H+HCO                                 8.00E+13    0.0        0.0
40. O+CH2(S)<=>H2+CO                              1.50E+13    0.0        0.0
41. O+CH2(S)<=>H+HCO                              1.50E+13    0.0        0.0
42. O+CH3<=>H+CH2O                                5.06E+13    0.0        0.0
43. O+CH4<=>OH+CH3                                1.02E+09    1.5     8600.0
44. O+CO(+M)<=>CO2(+M)                            1.80E+10    0.0     2385.0
    Low pressure limit:  0.60200E+15  0.00000E+00  0.30000E+04
    H2              Enhanced by    2.000E+00
    O2              Enhanced by    6.000E+00
    H2O             Enhanced by    6.000E+00
    CH4             Enhanced by    2.000E+00
    CO              Enhanced by    1.500E+00
    CO2             Enhanced by    3.500E+00
    C2H6            Enhanced by    3.000E+00
    AR              Enhanced by    5.000E-01
45. O+HCO<=>OH+CO                                 3.00E+13    0.0        0.0
46. O+HCO<=>H+CO2                                 3.00E+13    0.0        0.0
47. O+CH2O<=>OH+HCO                               3.90E+13    0.0     3540.0
48. O+CH2OH<=>OH+CH2O                             1.00E+13    0.0        0.0
49. O+CH3O<=>OH+CH2O                              1.00E+13    0.0        0.0
50. O+CH3OH<=>OH+CH2OH                            3.88E+05    2.5     3100.0
51. O+CH3OH<=>OH+CH3O                             1.30E+05    2.5     5000.0
52. O+C2H<=>CH+CO                                 5.00E+13    0.0        0.0
53. O+C2H2<=>H+HCCO                               1.35E+07    2.0     1900.0
54. O+C2H2<=>OH+C2H                               4.60E+19   -1.4    28950.0
55. O+C2H2<=>CO+CH2                               6.94E+06    2.0     1900.0
56. O+C2H3<=>H+CH2CO                              3.00E+13    0.0        0.0
57. O+C2H4<=>CH3+HCO                              1.25E+07    1.8      220.0
58. O+C2H5<=>CH3+CH2O                             2.24E+13    0.0        0.0
59. O+C2H6<=>OH+C2H5                              8.98E+07    1.9     5690.0
60. O+HCCO<=>H+2CO                                1.00E+14    0.0        0.0
61. O+CH2CO<=>OH+HCCO                             1.00E+13    0.0     8000.0
62. O+CH2CO<=>CH2+CO2                             1.75E+12    0.0     1350.0
63. O2+CO<=>O+CO2                                 2.50E+12    0.0    47800.0
64. O2+CH2O<=>HO2+HCO                             1.00E+14    0.0    40000.0
65. H+O2+M<=>HO2+M                                2.80E+18   -0.9        0.0
    O2              Enhanced by    0.000E+00
    H2O             Enhanced by    0.000E+00
```

```
    CO              Enhanced by    7.500E-01
    CO2             Enhanced by    1.500E+00
    C2H6            Enhanced by    1.500E+00
    N2              Enhanced by    0.000E+00
    AR              Enhanced by    0.000E+00
66. H+2O2<=>HO2+O2                          2.08E+19   -1.2        0.0
67. H+O2+H2O<=>HO2+H2O                      1.13E+19   -0.8        0.0
68. H+O2+N2<=>HO2+N2                        2.60E+19   -1.2        0.0
69. H+O2+AR<=>HO2+AR                        7.00E+17   -0.8        0.0
70. H+O2<=>O+OH                             2.65E+16   -0.7    17041.0
71. 2H+M<=>H2+M                             1.00E+18   -1.0        0.0
    H2              Enhanced by    0.000E+00
    H2O             Enhanced by    0.000E+00
    CH4             Enhanced by    2.000E+00
    CO2             Enhanced by    0.000E+00
    C2H6            Enhanced by    3.000E+00
    AR              Enhanced by    6.300E-01
72. 2H+H2<=>2H2                             9.00E+16   -0.6        0.0
73. 2H+H2O<=>H2+H2O                         6.00E+19   -1.2        0.0
74. 2H+CO2<=>H2+CO2                         5.50E+20   -2.0        0.0
75. H+OH+M<=>H2O+M                          2.20E+22   -2.0        0.0
    H2              Enhanced by    7.300E-01
    H2O             Enhanced by    3.650E+00
    CH4             Enhanced by    2.000E+00
    C2H6            Enhanced by    3.000E+00
    AR              Enhanced by    3.800E-01
76. H+HO2<=>O+H2O                           3.97E+12    0.0      671.0
77. H+HO2<=>O2+H2                           4.48E+13    0.0     1068.0
78. H+HO2<=>2OH                             8.40E+13    0.0      635.0
79. H+H2O2<=>HO2+H2                         1.21E+07    2.0     5200.0
80. H+H2O2<=>OH+H2O                         1.00E+13    0.0     3600.0
81. H+CH<=>C+H2                             1.65E+14    0.0        0.0
82. H+CH2(+M)<=>CH3(+M)                     6.00E+14    0.0        0.0
    Low pressure limit:  0.10400E+27 -0.27600E+01  0.16000E+04
    TROE centering:  0.56200E+00  0.91000E+02  0.58360E+04  0.85520E+04
    H2              Enhanced by    2.000E+00
    H2O             Enhanced by    6.000E+00
    CH4             Enhanced by    2.000E+00
    CO              Enhanced by    1.500E+00
    CO2             Enhanced by    2.000E+00
    C2H6            Enhanced by    3.000E+00
    AR              Enhanced by    7.000E-01
83. H+CH2(S)<=>CH+H2                        3.00E+13    0.0        0.0
84. H+CH3(+M)<=>CH4(+M)                     1.39E+16   -0.5      536.0
    Low pressure limit:  0.26200E+34 -0.47600E+01  0.24400E+04
    TROE centering:  0.78300E+00  0.74000E+02  0.29410E+04  0.69640E+04
    H2              Enhanced by    2.000E+00
    H2O             Enhanced by    6.000E+00
    CH4             Enhanced by    3.000E+00
    CO              Enhanced by    1.500E+00
    CO2             Enhanced by    2.000E+00
```

```
    C2H6            Enhanced by    3.000E+00
    AR              Enhanced by    7.000E-01
85. H+CH4<=>CH3+H2                          6.60E+08    1.6    10840.0
86. H+HCO(+M)<=>CH2O(+M)                    1.09E+12    0.5     -260.0
    Low pressure limit:  0.24700E+25 -0.25700E+01  0.42500E+03
    TROE centering:  0.78240E+00  0.27100E+03  0.27550E+04  0.65700E+04
    H2              Enhanced by    2.000E+00
    H2O             Enhanced by    6.000E+00
    CH4             Enhanced by    2.000E+00
    CO              Enhanced by    1.500E+00
    CO2             Enhanced by    2.000E+00
    C2H6            Enhanced by    3.000E+00
    AR              Enhanced by    7.000E-01
87. H+HCO<=>H2+CO                           7.34E+13    0.0        0.0
88. H+CH2O(+M)<=>CH2OH(+M)                  5.40E+11    0.5     3600.0
    Low pressure limit:  0.12700E+33 -0.48200E+01  0.65300E+04
    TROE centering:  0.71870E+00  0.10300E+03  0.12910E+04  0.41600E+04
    H2              Enhanced by    2.000E+00
    H2O             Enhanced by    6.000E+00
    CH4             Enhanced by    2.000E+00
    CO              Enhanced by    1.500E+00
    CO2             Enhanced by    2.000E+00
    C2H6            Enhanced by    3.000E+00
89. H+CH2O(+M)<=>CH3O(+M)                   5.40E+11    0.5     2600.0
    Low pressure limit:  0.22000E+31 -0.48000E+01  0.55600E+04
    TROE centering:  0.75800E+00  0.94000E+02  0.15550E+04  0.42000E+04
    H2              Enhanced by    2.000E+00
    H2O             Enhanced by    6.000E+00
    CH4             Enhanced by    2.000E+00
    CO              Enhanced by    1.500E+00
    CO2             Enhanced by    2.000E+00
    C2H6            Enhanced by    3.000E+00
90. H+CH2O<=>HCO+H2                         5.74E+07    1.9     2742.0
91. H+CH2OH(+M)<=>CH3OH(+M)                 1.06E+12    0.5       86.0
    Low pressure limit:  0.43600E+32 -0.46500E+01  0.50800E+04
    TROE centering:  0.60000E+00  0.10000E+03  0.90000E+05  0.10000E+05
    H2              Enhanced by    2.000E+00
    H2O             Enhanced by    6.000E+00
    CH4             Enhanced by    2.000E+00
    CO              Enhanced by    1.500E+00
    CO2             Enhanced by    2.000E+00
    C2H6            Enhanced by    3.000E+00
92. H+CH2OH<=>H2+CH2O                       2.00E+13    0.0        0.0
93. H+CH2OH<=>OH+CH3                        1.65E+11    0.7     -284.0
94. H+CH2OH<=>CH2(S)+H2O                    3.28E+13   -0.1      610.0
95. H+CH3O(+M)<=>CH3OH(+M)                  2.43E+12    0.5       50.0
    Low pressure limit:  0.46600E+42 -0.74400E+01  0.14080E+05
    TROE centering:  0.70000E+00  0.10000E+03  0.90000E+05  0.10000E+05
    H2              Enhanced by    2.000E+00
    H2O             Enhanced by    6.000E+00
    CH4             Enhanced by    2.000E+00
```

```
      CO              Enhanced by    1.500E+00
      CO2             Enhanced by    2.000E+00
      C2H6            Enhanced by    3.000E+00
  96. H+CH3O<=>H+CH2OH                         4.15E+07    1.6     1924.0
  97. H+CH3O<=>H2+CH2O                         2.00E+13    0.0        0.0
  98. H+CH3O<=>OH+CH3                          1.50E+12    0.5     -110.0
  99. H+CH3O<=>CH2(S)+H2O                      2.62E+14   -0.2     1070.0
 100. H+CH3OH<=>CH2OH+H2                       1.70E+07    2.1     4870.0
 101. H+CH3OH<=>CH3O+H2                        4.20E+06    2.1     4870.0
 102. H+C2H(+M)<=>C2H2(+M)                     1.00E+17   -1.0        0.0
      Low pressure limit:  0.37500E+34 -0.48000E+01  0.19000E+04
      TROE centering:  0.64640E+00  0.13200E+03  0.13150E+04  0.55660E+04
      H2              Enhanced by    2.000E+00
      H2O             Enhanced by    6.000E+00
      CH4             Enhanced by    2.000E+00
      CO              Enhanced by    1.500E+00
      CO2             Enhanced by    2.000E+00
      C2H6            Enhanced by    3.000E+00
      AR              Enhanced by    7.000E-01
 103. H+C2H2(+M)<=>C2H3(+M)                    5.60E+12    0.0     2400.0
      Low pressure limit:  0.38000E+41 -0.72700E+01  0.72200E+04
      TROE centering:  0.75070E+00  0.98500E+02  0.13020E+04  0.41670E+04
      H2              Enhanced by    2.000E+00
      H2O             Enhanced by    6.000E+00
      CH4             Enhanced by    2.000E+00
      CO              Enhanced by    1.500E+00
      CO2             Enhanced by    2.000E+00
      C2H6            Enhanced by    3.000E+00
      AR              Enhanced by    7.000E-01
 104. H+C2H3(+M)<=>C2H4(+M)                    6.08E+12    0.3      280.0
      Low pressure limit:  0.14000E+31 -0.38600E+01  0.33200E+04
      TROE centering:  0.78200E+00  0.20750E+03  0.26630E+04  0.60950E+04
      H2              Enhanced by    2.000E+00
      H2O             Enhanced by    6.000E+00
      CH4             Enhanced by    2.000E+00
      CO              Enhanced by    1.500E+00
      CO2             Enhanced by    2.000E+00
      C2H6            Enhanced by    3.000E+00
      AR              Enhanced by    7.000E-01
 105. H+C2H3<=>H2+C2H2                         3.00E+13    0.0        0.0
 106. H+C2H4(+M)<=>C2H5(+M)                         5.40E+11    0.5
1820.0
      Low pressure limit:  0.60000E+42 -0.76200E+01  0.69700E+04
      TROE centering:  0.97530E+00  0.21000E+03  0.98400E+03  0.43740E+04
      H2              Enhanced by    2.000E+00
      H2O             Enhanced by    6.000E+00
      CH4             Enhanced by    2.000E+00
      CO              Enhanced by    1.500E+00
      CO2             Enhanced by    2.000E+00
      C2H6            Enhanced by    3.000E+00
      AR              Enhanced by    7.000E-01
```

```
107. H+C2H4<=>C2H3+H2                          1.32E+06    2.5    12240.0
108. H+C2H5(+M)<=>C2H6(+M)                     5.21E+17   -1.0     1580.0
     Low pressure limit:  0.19900E+42 -0.70800E+01  0.66850E+04
     TROE centering:  0.84220E+00  0.12500E+03  0.22190E+04  0.68820E+04
     H2              Enhanced by    2.000E+00
     H2O             Enhanced by    6.000E+00
     CH4             Enhanced by    2.000E+00
     CO              Enhanced by    1.500E+00
     CO2             Enhanced by    2.000E+00
     C2H6            Enhanced by    3.000E+00
     AR              Enhanced by    7.000E-01
109. H+C2H5<=>H2+C2H4                          2.00E+12    0.0        0.0
110. H+C2H6<=>C2H5+H2                          1.15E+08    1.9     7530.0
111. H+HCCO<=>CH2(S)+CO                        1.00E+14    0.0        0.0
112. H+CH2CO<=>HCCO+H2                         5.00E+13    0.0     8000.0
113. H+CH2CO<=>CH3+CO                          1.13E+13    0.0     3428.0
114. H+HCCOH<=>H+CH2CO                         1.00E+13    0.0        0.0
115. H2+CO(+M)<=>CH2O(+M)                      4.30E+07    1.5    79600.0
     Low pressure limit:  0.50700E+28 -0.34200E+01  0.84350E+05
     TROE centering:  0.93200E+00  0.19700E+03  0.15400E+04  0.10300E+05
     H2              Enhanced by    2.000E+00
     H2O             Enhanced by    6.000E+00
     CH4             Enhanced by    2.000E+00
     CO              Enhanced by    1.500E+00
     CO2             Enhanced by    2.000E+00
     C2H6            Enhanced by    3.000E+00
     AR              Enhanced by    7.000E-01
116. OH+H2<=>H+H2O                             2.16E+08    1.5     3430.0
117. 2OH(+M)<=>H2O2(+M)                        7.40E+13   -0.4        0.0
     Low pressure limit:  0.23000E+19 -0.90000E+00 -0.17000E+04
     TROE centering:  0.73460E+00  0.94000E+02  0.17560E+04  0.51820E+04
     H2              Enhanced by    2.000E+00
     H2O             Enhanced by    6.000E+00
     CH4             Enhanced by    2.000E+00
     CO              Enhanced by    1.500E+00
     CO2             Enhanced by    2.000E+00
     C2H6            Enhanced by    3.000E+00
     AR              Enhanced by    7.000E-01
118. 2OH<=>O+H2O                               3.57E+04    2.4    -2110.0
119. OH+HO2<=>O2+H2O                           1.45E+13    0.0     -500.0
     Declared duplicate reaction...
120. OH+H2O2<=>HO2+H2O                         2.00E+12    0.0      427.0
     Declared duplicate reaction...
121. OH+H2O2<=>HO2+H2O                         1.70E+18    0.0    29410.0
     Declared duplicate reaction...
122. OH+C<=>H+CO                               5.00E+13    0.0        0.0
123. OH+CH<=>H+HCO                             3.00E+13    0.0        0.0
124. OH+CH2<=>H+CH2O                           2.00E+13    0.0        0.0
125. OH+CH2<=>CH+H2O                           1.13E+07    2.0     3000.0
126. OH+CH2(S)<=>H+CH2O                        3.00E+13    0.0        0.0
127. OH+CH3(+M)<=>CH3OH(+M)                    2.79E+18   -1.4     1330.0
```

```
     Low pressure limit:  0.40000E+37 -0.59200E+01  0.31400E+04
     TROE centering:  0.41200E+00  0.19500E+03  0.59000E+04  0.63940E+04
     H2              Enhanced by    2.000E+00
     H2O             Enhanced by    6.000E+00
     CH4             Enhanced by    2.000E+00
     CO              Enhanced by    1.500E+00
     CO2             Enhanced by    2.000E+00
     C2H6            Enhanced by    3.000E+00
128. OH+CH3<=>CH2+H2O                          5.60E+07    1.6     5420.0
129. OH+CH3<=>CH2(S)+H2O                       6.44E+17   -1.3     1417.0
130. OH+CH4<=>CH3+H2O                          1.00E+08    1.6     3120.0
131. OH+CO<=>H+CO2                             4.76E+07    1.2       70.0
132. OH+HCO<=>H2O+CO                           5.00E+13    0.0        0.0
133. OH+CH2O<=>HCO+H2O                         3.43E+09    1.2     -447.0
134. OH+CH2OH<=>H2O+CH2O                       5.00E+12    0.0        0.0
135. OH+CH3O<=>H2O+CH2O                        5.00E+12    0.0        0.0
136. OH+CH3OH<=>CH2OH+H2O                      1.44E+06    2.0     -840.0
137. OH+CH3OH<=>CH3O+H2O                       6.30E+06    2.0     1500.0
138. OH+C2H<=>H+HCCO                           2.00E+13    0.0        0.0
139. OH+C2H2<=>H+CH2CO                         2.18E-04    4.5    -1000.0
140. OH+C2H2<=>H+HCCOH                         5.04E+05    2.3    13500.0
141. OH+C2H2<=>C2H+H2O                         3.37E+07    2.0    14000.0
142. OH+C2H2<=>CH3+CO                          4.83E-04    4.0    -2000.0
143. OH+C2H3<=>H2O+C2H2                        5.00E+12    0.0        0.0
144. OH+C2H4<=>C2H3+H2O                        3.60E+06    2.0     2500.0
145. OH+C2H6<=>C2H5+H2O                        3.54E+06    2.1      870.0
146. OH+CH2CO<=>HCCO+H2O                       7.50E+12    0.0     2000.0
147. 2HO2<=>O2+H2O2                            1.30E+11    0.0    -1630.0
     Declared duplicate reaction...
148. 2HO2<=>O2+H2O2                            4.20E+14    0.0    12000.0
     Declared duplicate reaction...
149. HO2+CH2<=>OH+CH2O                         2.00E+13    0.0        0.0
150. HO2+CH3<=>O2+CH4                          1.00E+12    0.0        0.0
151. HO2+CH3<=>OH+CH3O                         3.78E+13    0.0        0.0
152. HO2+CO<=>OH+CO2                           1.50E+14    0.0    23600.0
153. HO2+CH2O<=>HCO+H2O2                       5.60E+06    2.0    12000.0
154. C+O2<=>O+CO                               5.80E+13    0.0      576.0
155. C+CH2<=>H+C2H                             5.00E+13    0.0        0.0
156. C+CH3<=>H+C2H2                            5.00E+13    0.0        0.0
157. CH+O2<=>O+HCO                             6.71E+13    0.0        0.0
158. CH+H2<=>H+CH2                             1.08E+14    0.0     3110.0
159. CH+H2O<=>H+CH2O                           5.71E+12    0.0     -755.0
160. CH+CH2<=>H+C2H2                           4.00E+13    0.0        0.0
161. CH+CH3<=>H+C2H3                           3.00E+13    0.0        0.0
162. CH+CH4<=>H+C2H4                           6.00E+13    0.0        0.0
163. CH+CO(+M)<=>HCCO(+M)                      5.00E+13    0.0        0.0
     Low pressure limit:  0.26900E+29 -0.37400E+01  0.19360E+04
     TROE centering:  0.57570E+00  0.23700E+03  0.16520E+04  0.50690E+04
     H2              Enhanced by    2.000E+00
     H2O             Enhanced by    6.000E+00
     CH4             Enhanced by    2.000E+00
```

```
     CO              Enhanced by    1.500E+00
     CO2             Enhanced by    2.000E+00
     C2H6            Enhanced by    3.000E+00
     AR              Enhanced by    7.000E-01
164. CH+CO2<=>HCO+CO                          1.90E+14    0.0    15792.0
165. CH+CH2O<=>H+CH2CO                        9.46E+13    0.0     -515.0
166. CH+HCCO<=>CO+C2H2                        5.00E+13    0.0        0.0
167. CH2+O2=>OH+H+CO                          5.00E+12    0.0     1500.0
168. CH2+H2<=>H+CH3                           5.00E+05    2.0     7230.0
169. 2CH2<=>H2+C2H2                           1.60E+15    0.0    11944.0
170. CH2+CH3<=>H+C2H4                         4.00E+13    0.0        0.0
171. CH2+CH4<=>2CH3                           2.46E+06    2.0     8270.0
172. CH2+CO(+M)<=>CH2CO(+M)                   8.10E+11    0.5     4510.0
     Low pressure limit:  0.26900E+34 -0.51100E+01  0.70950E+04
     TROE centering:  0.59070E+00  0.27500E+03  0.12260E+04  0.51850E+04
     H2              Enhanced by    2.000E+00
     H2O             Enhanced by    6.000E+00
     CH4             Enhanced by    2.000E+00
     CO              Enhanced by    1.500E+00
     CO2             Enhanced by    2.000E+00
     C2H6            Enhanced by    3.000E+00
     AR              Enhanced by    7.000E-01
173. CH2+HCCO<=>C2H3+CO                       3.00E+13    0.0        0.0
174. CH2(S)+N2<=>CH2+N2                       1.50E+13    0.0      600.0
175. CH2(S)+AR<=>CH2+AR                       9.00E+12    0.0      600.0
176. CH2(S)+O2<=>H+OH+CO                      2.80E+13    0.0        0.0
177. CH2(S)+O2<=>CO+H2O                       1.20E+13    0.0        0.0
178. CH2(S)+H2<=>CH3+H                        7.00E+13    0.0        0.0
179. CH2(S)+H2O(+M)<=>CH3OH(+M)               4.82E+17   -1.2     1145.0
     Low pressure limit:  0.18800E+39 -0.63600E+01  0.50400E+04
     TROE centering:  0.60270E+00  0.20800E+03  0.39220E+04  0.10180E+05
     H2              Enhanced by    2.000E+00
     H2O             Enhanced by    6.000E+00
     CH4             Enhanced by    2.000E+00
     CO              Enhanced by    1.500E+00
     CO2             Enhanced by    2.000E+00
     C2H6            Enhanced by    3.000E+00
180. CH2(S)+H2O<=>CH2+H2O                     3.00E+13    0.0        0.0
181. CH2(S)+CH3<=>H+C2H4                      1.20E+13    0.0     -570.0
182. CH2(S)+CH4<=>2CH3                        1.60E+13    0.0     -570.0
183. CH2(S)+CO<=>CH2+CO                       9.00E+12    0.0        0.0
184. CH2(S)+CO2<=>CH2+CO2                     7.00E+12    0.0        0.0
185. CH2(S)+CO2<=>CO+CH2O                     1.40E+13    0.0        0.0
186. CH2(S)+C2H6<=>CH3+C2H5                   4.00E+13    0.0     -550.0
187. CH3+O2<=>O+CH3O                          3.56E+13    0.0    30480.0
188. CH3+O2<=>OH+CH2O                         2.31E+12    0.0    20315.0
189. CH3+H2O2<=>HO2+CH4                       2.45E+04    2.5     5180.0
190. 2CH3(+M)<=>C2H6(+M)                      6.77E+16   -1.2      654.0
     Low pressure limit:  0.34000E+42 -0.70300E+01  0.27620E+04
     TROE centering:  0.61900E+00  0.73200E+02  0.11800E+04  0.99990E+04
     H2              Enhanced by    2.000E+00
```

```
     H2O             Enhanced by    6.000E+00
     CH4             Enhanced by    2.000E+00
     CO              Enhanced by    1.500E+00
     CO2             Enhanced by    2.000E+00
     C2H6            Enhanced by    3.000E+00
     AR              Enhanced by    7.000E-01
191. 2CH3<=>H+C2H5                              6.84E+12    0.1    10600.0
192. CH3+HCO<=>CH4+CO                           2.65E+13    0.0        0.0
193. CH3+CH2O<=>HCO+CH4                         3.32E+03    2.8     5860.0
194. CH3+CH3OH<=>CH2OH+CH4                      3.00E+07    1.5     9940.0
195. CH3+CH3OH<=>CH3O+CH4                       1.00E+07    1.5     9940.0
196. CH3+C2H4<=>C2H3+CH4                        2.27E+05    2.0     9200.0
197. CH3+C2H6<=>C2H5+CH4                        6.14E+06    1.7    10450.0
198. HCO+H2O<=>H+CO+H2O                         1.50E+18   -1.0    17000.0
199. HCO+M<=>H+CO+M                             1.87E+17   -1.0    17000.0
     H2              Enhanced by    2.000E+00
     H2O             Enhanced by    0.000E+00
     CH4             Enhanced by    2.000E+00
     CO              Enhanced by    1.500E+00
     CO2             Enhanced by    2.000E+00
     C2H6            Enhanced by    3.000E+00
200. HCO+O2<=>HO2+CO                            1.34E+13    0.0      400.0
201. CH2OH+O2<=>HO2+CH2O                        1.80E+13    0.0      900.0
202. CH3O+O2<=>HO2+CH2O                         4.28E-13    7.6    -3530.0
203. C2H+O2<=>HCO+CO                            1.00E+13    0.0     -755.0
204. C2H+H2<=>H+C2H2                            5.68E+10    0.9     1993.0
205. C2H3+O2<=>HCO+CH2O                         4.58E+16   -1.4     1015.0
206. C2H4(+M)<=>H2+C2H2(+M)                     8.00E+12    0.4    86770.0
     Low pressure limit:  0.15800E+52 -0.93000E+01  0.97800E+05
     TROE centering:  0.73450E+00  0.18000E+03  0.10350E+04  0.54170E+04
     H2              Enhanced by    2.000E+00
     H2O             Enhanced by    6.000E+00
     CH4             Enhanced by    2.000E+00
     CO              Enhanced by    1.500E+00
     CO2             Enhanced by    2.000E+00
     C2H6            Enhanced by    3.000E+00
     AR              Enhanced by    7.000E-01
207. C2H5+O2<=>HO2+C2H4                         8.40E+11    0.0     3875.0
208. HCCO+O2<=>OH+2CO                           3.20E+12    0.0      854.0
209. 2HCCO<=>2CO+C2H2                           1.00E+13    0.0        0.0
210. N+NO<=>N2+O                                2.70E+13    0.0      355.0
211. N+O2<=>NO+O                                9.00E+09    1.0     6500.0
212. N+OH<=>NO+H                                3.36E+13    0.0      385.0
213. N2O+O<=>N2+O2                              1.40E+12    0.0    10810.0
214. N2O+O<=>2NO                                2.90E+13    0.0    23150.0
215. N2O+H<=>N2+OH                              3.87E+14    0.0    18880.0
216. N2O+OH<=>N2+HO2                            2.00E+12    0.0    21060.0
217. N2O(+M)<=>N2+O(+M)                         7.91E+10    0.0    56020.0
     Low pressure limit:  0.63700E+15  0.00000E+00  0.56640E+05
     H2              Enhanced by    2.000E+00
     H2O             Enhanced by    6.000E+00
```

```
     CH4             Enhanced by    2.000E+00
     CO              Enhanced by    1.500E+00
     CO2             Enhanced by    2.000E+00
     C2H6            Enhanced by    3.000E+00
     AR              Enhanced by    6.250E-01
218. HO2+NO<=>NO2+OH                          2.11E+12    0.0     -480.0
219. NO+O+M<=>NO2+M                           1.06E+20   -1.4        0.0
     H2              Enhanced by    2.000E+00
     H2O             Enhanced by    6.000E+00
     CH4             Enhanced by    2.000E+00
     CO              Enhanced by    1.500E+00
     CO2             Enhanced by    2.000E+00
     C2H6            Enhanced by    3.000E+00
     AR              Enhanced by    7.000E-01
220. NO2+O<=>NO+O2                            3.90E+12    0.0     -240.0
221. NO2+H<=>NO+OH                            1.32E+14    0.0      360.0
222. NH+O<=>NO+H                              4.00E+13    0.0        0.0
223. NH+H<=>N+H2                              3.20E+13    0.0      330.0
224. NH+OH<=>HNO+H                            2.00E+13    0.0        0.0
225. NH+OH<=>N+H2O                            2.00E+09    1.2        0.0
226. NH+O2<=>HNO+O                            4.61E+05    2.0     6500.0
227. NH+O2<=>NO+OH                            1.28E+06    1.5      100.0
228. NH+N<=>N2+H                              1.50E+13    0.0        0.0
229. NH+H2O<=>HNO+H2                          2.00E+13    0.0    13850.0
230. NH+NO<=>N2+OH                            2.16E+13   -0.2        0.0
231. NH+NO<=>N2O+H                            3.65E+14   -0.5        0.0
232. NH2+O<=>OH+NH                            3.00E+12    0.0        0.0
233. NH2+O<=>H+HNO                            3.90E+13    0.0        0.0
234. NH2+H<=>NH+H2                            4.00E+13    0.0     3650.0
235. NH2+OH<=>NH+H2O                          9.00E+07    1.5     -460.0
236. NNH<=>N2+H                               3.30E+08    0.0        0.0
237. NNH+M<=>N2+H+M                           1.30E+14   -0.1     4980.0
     H2              Enhanced by    2.000E+00
     H2O             Enhanced by    6.000E+00
     CH4             Enhanced by    2.000E+00
     CO              Enhanced by    1.500E+00
     CO2             Enhanced by    2.000E+00
     C2H6            Enhanced by    3.000E+00
     AR              Enhanced by    7.000E-01
238. NNH+O2<=>HO2+N2                          5.00E+12    0.0        0.0
239. NNH+O<=>OH+N2                            2.50E+13    0.0        0.0
240. NNH+O<=>NH+NO                            7.00E+13    0.0        0.0
241. NNH+H<=>H2+N2                            5.00E+13    0.0        0.0
242. NNH+OH<=>H2O+N2                          2.00E+13    0.0        0.0
243. NNH+CH3<=>CH4+N2                         2.50E+13    0.0        0.0
244. H+NO+M<=>HNO+M                           4.48E+19   -1.3      740.0
     H2              Enhanced by    2.000E+00
     H2O             Enhanced by    6.000E+00
     CH4             Enhanced by    2.000E+00
     CO              Enhanced by    1.500E+00
     CO2             Enhanced by    2.000E+00
```

```
     C2H6            Enhanced by    3.000E+00
     AR              Enhanced by    7.000E-01
245. HNO+O<=>NO+OH                              2.50E+13    0.0        0.0
246. HNO+H<=>H2+NO                              9.00E+11    0.7      660.0
247. HNO+OH<=>NO+H2O                            1.30E+07    1.9     -950.0
248. HNO+O2<=>HO2+NO                            1.00E+13    0.0    13000.0
249. CN+O<=>CO+N                                7.70E+13    0.0        0.0
250. CN+OH<=>NCO+H                              4.00E+13    0.0        0.0
251. CN+H2O<=>HCN+OH                            8.00E+12    0.0     7460.0
252. CN+O2<=>NCO+O                              6.14E+12    0.0     -440.0
253. CN+H2<=>HCN+H                              2.95E+05    2.5     2240.0
254. NCO+O<=>NO+CO                              2.35E+13    0.0        0.0
255. NCO+H<=>NH+CO                              5.40E+13    0.0        0.0
256. NCO+OH<=>NO+H+CO                           2.50E+12    0.0        0.0
257. NCO+N<=>N2+CO                              2.00E+13    0.0        0.0
258. NCO+O2<=>NO+CO2                            2.00E+12    0.0    20000.0
259. NCO+M<=>N+CO+M                             3.10E+14    0.0    54050.0
     H2              Enhanced by    2.000E+00
     H2O             Enhanced by    6.000E+00
     CH4             Enhanced by    2.000E+00
     CO              Enhanced by    1.500E+00
     CO2             Enhanced by    2.000E+00
     C2H6            Enhanced by    3.000E+00
     AR              Enhanced by    7.000E-01
260. NCO+NO<=>N2O+CO                            1.90E+17   -1.5      740.0
261. NCO+NO<=>N2+CO2                            3.80E+18   -2.0      800.0
262. HCN+M<=>H+CN+M                             1.04E+29   -3.3   126600.0
     H2              Enhanced by    2.000E+00
     H2O             Enhanced by    6.000E+00
     CH4             Enhanced by    2.000E+00
     CO              Enhanced by    1.500E+00
     CO2             Enhanced by    2.000E+00
     C2H6            Enhanced by    3.000E+00
     AR              Enhanced by    7.000E-01
263. HCN+O<=>NCO+H                          2.03E+04    2.6     4980.0
264. HCN+O<=>NH+CO                          5.07E+03    2.6     4980.0
265. HCN+O<=>CN+OH                          3.91E+09    1.6    26600.0
266. HCN+OH<=>HOCN+H                        1.10E+06    2.0    13370.0
267. HCN+OH<=>HNCO+H                        4.40E+03    2.3     6400.0
268. HCN+OH<=>NH2+CO                        1.60E+02    2.6     9000.0
269. H+HCN(+M)<=>H2CN(+M)                   3.30E+13    0.0        0.0
     Low pressure limit:  0.14000E+27 -0.34000E+01  0.19000E+04
     H2              Enhanced by    2.000E+00
     H2O             Enhanced by    6.000E+00
     CH4             Enhanced by    2.000E+00
     CO              Enhanced by    1.500E+00
     CO2             Enhanced by    2.000E+00
     C2H6            Enhanced by    3.000E+00
     AR              Enhanced by    7.000E-01
270. H2CN+N<=>N2+CH2                        6.00E+13    0.0      400.0
271. C+N2<=>CN+N                            6.30E+13    0.0    46020.0
```

```
272. CH+N2<=>HCN+N                                3.12E+09    0.9    20130.0
273. CH+N2(+M)<=>HCNN(+M)                         3.10E+12    0.1        0.0
     Low pressure limit:  0.13000E+26 -0.31600E+01  0.74000E+03
     TROE centering:  0.66700E+00  0.23500E+03  0.21170E+04  0.45360E+04
     H2              Enhanced by    2.000E+00
     H2O             Enhanced by    6.000E+00
     CH4             Enhanced by    2.000E+00
     CO              Enhanced by    1.500E+00
     CO2             Enhanced by    2.000E+00
     C2H6            Enhanced by    3.000E+00
     AR              Enhanced by    1.000E+00
274. CH2+N2<=>HCN+NH                              1.00E+13    0.0    74000.0
275. CH2(S)+N2<=>NH+HCN                           1.00E+11    0.0    65000.0
276. C+NO<=>CN+O                                  1.90E+13    0.0        0.0
277. C+NO<=>CO+N                                  2.90E+13    0.0        0.0
278. CH+NO<=>HCN+O                                4.10E+13    0.0        0.0
279. CH+NO<=>H+NCO                                1.62E+13    0.0        0.0
280. CH+NO<=>N+HCO                                2.46E+13    0.0        0.0
281. CH2+NO<=>H+HNCO                              3.10E+17   -1.4     1270.0
282. CH2+NO<=>OH+HCN                              2.90E+14   -0.7      760.0
283. CH2+NO<=>H+HCNO                              3.80E+13   -0.4      580.0
284. CH2(S)+NO<=>H+HNCO                           3.10E+17   -1.4     1270.0
285. CH2(S)+NO<=>OH+HCN                           2.90E+14   -0.7      760.0
286. CH2(S)+NO<=>H+HCNO                           3.80E+13   -0.4      580.0
287. CH3+NO<=>HCN+H2O                             9.60E+13    0.0    28800.0
288. CH3+NO<=>H2CN+OH                             1.00E+12    0.0    21750.0
289. HCNN+O<=>CO+H+N2                             2.20E+13    0.0        0.0
290. HCNN+O<=>HCN+NO                              2.00E+12    0.0        0.0
291. HCNN+O2<=>O+HCO+N2                           1.20E+13    0.0        0.0
292. HCNN+OH<=>H+HCO+N2                           1.20E+13    0.0        0.0
293. HCNN+H<=>CH2+N2                              1.00E+14    0.0        0.0
294. HNCO+O<=>NH+CO2                              9.80E+07    1.4     8500.0
295. HNCO+O<=>HNO+CO                              1.50E+08    1.6    44000.0
296. HNCO+O<=>NCO+OH                              2.20E+06    2.1    11400.0
297. HNCO+H<=>NH2+CO                              2.25E+07    1.7     3800.0
298. HNCO+H<=>H2+NCO                              1.05E+05    2.5    13300.0
299. HNCO+OH<=>NCO+H2O                            3.30E+07    1.5     3600.0
300. HNCO+OH<=>NH2+CO2                            3.30E+06    1.5     3600.0
301. HNCO+M<=>NH+CO+M                             1.18E+16    0.0    84720.0
     H2              Enhanced by    2.000E+00
     H2O             Enhanced by    6.000E+00
     CH4             Enhanced by    2.000E+00
     CO              Enhanced by    1.500E+00
     CO2             Enhanced by    2.000E+00
     C2H6            Enhanced by    3.000E+00
     AR              Enhanced by    7.000E-01
302. HCNO+H<=>H+HNCO                              2.10E+15   -0.7     2850.0
303. HCNO+H<=>OH+HCN                              2.70E+11    0.2     2120.0
304. HCNO+H<=>NH2+CO                              1.70E+14   -0.8     2890.0
305. HOCN+H<=>H+HNCO                              2.00E+07    2.0     2000.0
306. HCCO+NO<=>HCNO+CO                            9.00E+12    0.0        0.0
```

```
307. CH3+N<=>H2CN+H                                6.10E+14   -0.3      290.0
308. CH3+N<=>HCN+H2                                3.70E+12    0.1      -90.0
309. NH3+H<=>NH2+H2                                5.40E+05    2.4     9915.0
310. NH3+OH<=>NH2+H2O                              5.00E+07    1.6      955.0
311. NH3+O<=>NH2+OH                                9.40E+06    1.9     6460.0
312. NH+CO2<=>HNO+CO                               1.00E+13    0.0    14350.0
313. CN+NO2<=>NCO+NO                               6.16E+15   -0.8      345.0
314. NCO+NO2<=>N2O+CO2                             3.25E+12    0.0     -705.0
315. N+CO2<=>NO+CO                                 3.00E+12    0.0    11300.0
316. O+CH3=>H+H2+CO                                3.37E+13    0.0        0.0
317. O+C2H4<=>H+CH2CHO                             6.70E+06    1.8      220.0
318. O+C2H5<=>H+CH3CHO                             1.10E+14    0.0        0.0
319. OH+HO2<=>O2+H2O                               5.00E+15    0.0    17330.0
     Declared duplicate reaction...
320. OH+CH3=>H2+CH2O                               8.00E+09    0.5    -1755.0
321. CH+H2(+M)<=>CH3(+M)                           1.97E+12    0.4     -370.0
     Low pressure limit:  0.48200E+26 -0.28000E+01  0.59000E+03
     TROE centering:  0.57800E+00  0.12200E+03  0.25350E+04  0.93650E+04
     H2              Enhanced by    2.000E+00
     H2O             Enhanced by    6.000E+00
     CH4             Enhanced by    2.000E+00
     CO              Enhanced by    1.500E+00
     CO2             Enhanced by    2.000E+00
     C2H6            Enhanced by    3.000E+00
     AR              Enhanced by    7.000E-01
322. CH2+O2=>2H+CO2                                5.80E+12    0.0     1500.0
323. CH2+O2<=>O+CH2O                               2.40E+12    0.0     1500.0
324. CH2+CH2=>2H+C2H2                              2.00E+14    0.0    10989.0
325. CH2(S)+H2O=>H2+CH2O                           6.82E+10    0.2     -935.0
326. C2H3+O2<=>O+CH2CHO                            3.03E+11    0.3       11.0
327. C2H3+O2<=>HO2+C2H2                            1.34E+06    1.6     -384.0
328. O+CH3CHO<=>OH+CH2CHO                          2.92E+12    0.0     1808.0
329. O+CH3CHO=>OH+CH3+CO                           2.92E+12    0.0     1808.0
330. O2+CH3CHO=>HO2+CH3+CO                         3.01E+13    0.0    39150.0
331. H+CH3CHO<=>CH2CHO+H2                          2.05E+09    1.2     2405.0
332. H+CH3CHO=>CH3+H2+CO                           2.05E+09    1.2     2405.0
333. OH+CH3CHO=>CH3+H2O+CO                         2.34E+10    0.7    -1113.0
334. HO2+CH3CHO=>CH3+H2O2+CO                       3.01E+12    0.0    11923.0
335. CH3+CH3CHO=>CH3+CH4+CO                        2.72E+06    1.8     5920.0
336. H+CH2CO(+M)<=>CH2CHO(+M)                      4.86E+11    0.4    -1755.0
     Low pressure limit:  0.10120E+43 -0.76300E+01  0.38540E+04
     TROE centering:  0.46500E+00  0.20100E+03  0.17730E+04  0.53330E+04
     H2              Enhanced by    2.000E+00
     H2O             Enhanced by    6.000E+00
     CH4             Enhanced by    2.000E+00
     CO              Enhanced by    1.500E+00
     CO2             Enhanced by    2.000E+00
     C2H6            Enhanced by    3.000E+00
     AR              Enhanced by    7.000E-01
337. O+CH2CHO=>H+CH2+CO2                           1.50E+14    0.0        0.0
338. O2+CH2CHO=>OH+CO+CH2O                         1.81E+10    0.0        0.0
```

```
 339. O2+CH2CHO=>OH+2HCO                          2.35E+10    0.0        0.0
 340. H+CH2CHO<=>CH3+HCO                          2.20E+13    0.0        0.0
 341. H+CH2CHO<=>CH2CO+H2                         1.10E+13    0.0        0.0
 342. OH+CH2CHO<=>H2O+CH2CO                       1.20E+13    0.0        0.0
 343. OH+CH2CHO<=>HCO+CH2OH                       3.01E+13    0.0        0.0
 344. CH3+C2H5(+M)<=>C3H8(+M)                     9.43E+12    0.0        0.0
      Low pressure limit:  0.27100E+75 -0.16820E+02  0.13065E+05
      TROE centering:      0.15270E+00  0.29100E+03  0.27420E+04
0.77480E+04
      H2              Enhanced by    2.000E+00
      H2O             Enhanced by    6.000E+00
      CH4             Enhanced by    2.000E+00
      CO              Enhanced by    1.500E+00
      CO2             Enhanced by    2.000E+00
      C2H6            Enhanced by    3.000E+00
      AR              Enhanced by    7.000E-01
 345. O+C3H8<=>OH+C3H7                            1.93E+05    2.7     3716.0
 346. H+C3H8<=>C3H7+H2                            1.32E+06    2.5     6756.0
 347. OH+C3H8<=>C3H7+H2O                          3.16E+07    1.8      934.0
 348. C3H7+H2O2<=>HO2+C3H8                        3.78E+02    2.7     1500.0
 349. CH3+C3H8<=>C3H7+CH4                         9.03E-01    3.6     7154.0
 350. CH3+C2H4(+M)<=>C3H7(+M)                     2.55E+06    1.6     5700.0
      Low pressure limit:  0.30000E+64 -0.14600E+02  0.18170E+05
      TROE centering:      0.18940E+00  0.27700E+03  0.87480E+04
0.78910E+04
      H2              Enhanced by    2.000E+00
      H2O             Enhanced by    6.000E+00
      CH4             Enhanced by    2.000E+00
      CO              Enhanced by    1.500E+00
      CO2             Enhanced by    2.000E+00
      C2H6            Enhanced by    3.000E+00
      AR              Enhanced by    7.000E-01
 351. O+C3H7<=>C2H5+CH2O                          9.64E+13    0.0        0.0
 352. H+C3H7(+M)<=>C3H8(+M)                       3.61E+13    0.0        0.0
      Low pressure limit:  0.44200E+62 -0.13545E+02  0.11357E+05
      TROE centering:      0.31500E+00  0.36900E+03  0.32850E+04
0.66670E+04
      H2              Enhanced by    2.000E+00
      H2O             Enhanced by    6.000E+00
      CH4             Enhanced by    2.000E+00
      CO              Enhanced by    1.500E+00
      CO2             Enhanced by    2.000E+00
      C2H6            Enhanced by    3.000E+00
      AR              Enhanced by    7.000E-01
 353. H+C3H7<=>CH3+C2H5                           4.06E+06    2.2      890.0
 354. OH+C3H7<=>C2H5+CH2OH                        2.41E+13    0.0        0.0
 355. HO2+C3H7<=>O2+C3H8                          2.55E+10    0.3     -943.0
 356. HO2+C3H7=>OH+C2H5+CH2O                      2.41E+13    0.0        0.0
 357. CH3+C3H7<=>2C2H5                            1.93E+13   -0.3        0.0

  NOTE: A units mole-cm-sec-K, E units cal/mole
```

VITA

Name:	Nicole Donato
Address:	Dr. Eric Petersen Department of Mechanical Engineering 3123 TAMU College Station, TX 77843-3123
Email Address:	Nicole.S.Donato@gmail.com
Education:	B.S. Aerospace Engineering, University of Central Florida, 2003 M.S. Mechanical Engineering, Texas A&M University, 2009